Atmospheric
Chemistry
and Physics

Secondary organic aerosol formation from in situ OH, O₃, and NO₃ oxidation of ambient forest air in an oxidation flow reactor

Brett B. Palm[1,2], Pedro Campuzano-Jost[1,2], Douglas A. Day[1,2], Amber M. Ortega[1,3,a], Juliane L. Fry[4],
Steven S. Brown[2,5], Kyle J. Zarzana[1,2,b], William Dube[1,5], Nicholas L. Wagner[1,5], Danielle C. Draper[4,c], Lisa Kaser[6],
Werner Jud[7,d], Thomas Karl[8], Armin Hansel[7], Cándido Gutiérrez-Montes[9], and Jose L. Jimenez[1,2]

[1]Cooperative Institute for Research in Environmental Sciences, University of Colorado, Boulder, CO, USA
[2]Department of Chemistry and Biochemistry, University of Colorado, Boulder, CO, USA
[3]Department of Atmospheric and Oceanic Science, University of Colorado, Boulder, CO, USA
[4]Department of Chemistry, Reed College, Portland, OR, USA
[5]NOAA Earth System Research Laboratory, Chemical Sciences Division, Boulder, CO, USA
[6]Atmospheric Chemistry Observations & Modeling Laboratory, National Center for Atmospheric Research,
Boulder, CO, USA
[7]Institute of Ion Physics and Applied Physics, University of Innsbruck, Austria
[8]Institute of Atmospheric and Cryospheric Sciences, University of Innsbruck, Austria
[9]Departamento de Ingeniería, Mecánica y Minera, Universidad de Jaen, Jaen, Spain
[a]now at: Air Pollution Control Division, Colorado Department of Public Health and Environment, Denver, CO, USA
[b]now at: NOAA Earth System Research Laboratory, Chemical Sciences Division, Boulder, CO, USA
[c]now at: Department of Chemistry, University of California, Irvine, USA
[d]now at: Research Unit Environmental Simulation (EUS), Institute of Biochemical Plant Pathology (BIOP), Helmholtz
Zentrum München GmbH, Oberschleißheim, Germany

Correspondence to: Jose L. Jimenez (jose.jimenez@colorado.edu)

Abstract. Ambient pine forest air was oxidized by OH, O₃, or NO₃ radicals using an oxidation flow reactor (OFR) during the BEACHON-RoMBAS (Bio–hydro–atmosphere interactions of Energy, Aerosols, Carbon, H₂O, Organics and Nitrogen – Rocky Mountain Biogenic Aerosol Study) campaign to study biogenic secondary organic aerosol (SOA) formation and organic aerosol (OA) aging. A wide range of equivalent atmospheric photochemical ages was sampled, from hours up to days (for O₃ and NO₃) or weeks (for OH). Ambient air processed by the OFR was typically sampled every 20–30 min, in order to determine how the availability of SOA precursor gases in ambient air changed with diurnal and synoptic conditions, for each of the three oxidants. More SOA was formed during nighttime than daytime for all three oxidants, indicating that SOA precursor concentrations were higher at night. At all times of day, OH oxidation led to approximately 4 times more SOA formation than either O₃ or NO₃ oxidation. This is likely because O₃ and NO₃ will only react with gases containing $C = C$ bonds (e.g., terpenes) to form SOA but will not react appreciably with many of their oxidation products or any species in the gas phase that lacks a $C = C$ bond (e.g., pinonic acid, alkanes). In contrast, OH can continue to react with compounds that lack $C = C$ bonds to produce SOA. Closure was achieved between the amount of SOA formed from O₃ and NO₃ oxidation in the OFR and the SOA predicted to form from measured concentrations of ambient monoterpenes and sesquiterpenes using published chamber yields. This is in contrast to previous work at this site (Palm et al., 2016), which has shown that a source of SOA from semi- and intermediate-volatility organic compounds (S/IVOCs) 3.4 times larger than the source from measured VOCs is needed to explain the measured SOA formation from OH oxidation. This work suggests that those S/IVOCs typically do not contain $C = C$ bonds. O₃ and NO₃

oxidation produced SOA with elemental O : C and H : C similar to the least-oxidized OA observed in local ambient air, and neither oxidant led to net mass loss at the highest exposures, in contrast to OH oxidation. An OH exposure in the OFR equivalent to several hours of atmospheric aging also produced SOA with O : C and H : C values similar to ambient OA, while higher aging (days–weeks) led to formation of SOA with progressively higher O : C and lower H : C (and net mass loss at the highest exposures). NO$_3$ oxidation led to the production of particulate organic nitrates (pRONO$_2$), while OH and O$_3$ oxidation (under low NO) did not, as expected. These measurements of SOA formation provide the first direct comparison of SOA formation potential and chemical evolution from OH, O$_3$, and NO$_3$ oxidation in the real atmosphere and help to clarify the oxidation processes that lead to SOA formation from biogenic hydrocarbons.

1 Introduction

Submicron atmospheric aerosols have important impacts on radiative climate forcing (Myhre et al., 2013) and human health (Pope and Dockery, 2006). A large fraction of submicron particulate mass is composed of organic aerosols (OA) and is produced from a variety of sources (Zhang et al., 2007). Primary OA (POA) is directly emitted as particles (e.g., via fossil fuel combustion, biomass burning), while secondary OA (SOA) can be formed through gas-phase oxidation and gas-to-particle conversion of directly emitted organic gases or via aqueous pathways. Globally, SOA comprises the majority of OA, particularly in rural locations away from primary sources (Zhang et al., 2007; Jimenez et al., 2009). However, the processes of formation, chemical transformation, and removal of SOA remain uncertain (Hallquist et al., 2009; Shrivastava et al., 2016).

Hydroxyl radicals (OH), ozone (O$_3$), and nitrate radicals (NO$_3$) are the three major oxidants in the atmosphere that react with organic gases to form SOA. The initial steps of oxidation for each oxidant are summarized here according to Atkinson and Arey (2003):

– OH can react via H abstraction or addition to a C = C double bond, depending on the structure of the organic molecule.

– O$_3$ generally reacts only with alkenes, adding to a C = C bond to produce a primary ozonide, which then decomposes to form a carbonyl plus a Criegee intermediate.

– NO$_3$ radicals also react by addition to a C = C bond, producing an organic peroxy radical with an adjacent organic nitrate group that will react further. The nitrate functional group formed during the initial NO$_3$ addition can either remain in the product molecule or decompose to produce NO$_2$ (g).

Nearly all oxidation pathways in the atmosphere will lead to the production of a peroxy radical (RO$_2$), which can proceed to react with HO$_2$, NO$_2$, NO, another RO$_2$, or undergo autoxidation (Atkinson, 1997; Orlando and Tyndall, 2012; Crounse et al., 2013). Reaction rate constants and more detailed reaction mechanisms can be found elsewhere (e.g., Atkinson et al., 1982; Atkinson, 1997; Chew et al., 1998; Calvert et al., 2002).

SOA yields from the oxidation of a wide variety of precursor gases by each of these three oxidants have been reported. SOA yields are typically measured from oxidation experiments in large environmental chambers. These yields are evaluated through implementation in regional or global models, which can be compared to ambient measurements (e.g., Volkamer et al., 2006; Hayes et al., 2015). However, large chamber experiments have been shown to be affected by large losses of semivolatile and low-volatility gases (Matsunaga and Ziemann, 2010; Zhang et al., 2014; Krechmer et al., 2015; La et al., 2016; Nah et al., 2016) and particles (Crump and Seinfeld, 1981; McMurry and Rader, 1985; Pierce et al., 2008) to the chamber walls. These artifacts affect the ability to accurately measure SOA yields and also limit the amount of oxidation that can be achieved in chambers. Large variability in OA concentrations exists between various global OA models, which typically achieve poor agreement and correlation with ambient surface and vertical profile OA concentration measurements (Tsigaridis et al., 2014).

In addition to bulk concentrations, the chemical composition of OA also determines its atmospheric properties. The elemental O : C and H : C ratios of OA can be measured using aerosol mass spectrometry (Aiken et al., 2008; Canagaratna et al., 2015). The O : C and H : C ratios can provide information about the sources and evolution of OA in the atmosphere (Aiken et al., 2008; Heald et al., 2010; Kroll et al., 2011; Ng et al., 2011) and also often correlate with key OA properties such as hygroscopicity, material density, and phase separation (Jimenez et al., 2009; Bertram et al., 2011; Kuwata et al., 2012). Laboratory studies have typically struggled to reproduce the O : C and H : C values found in ambient OA, particularly for the highest O : C values found in remote areas (Aiken et al., 2008; Chen et al., 2015).

While large chambers have been the standard method for studying SOA yields and composition and are the basis for parameterized yields and oxidation in most models, oxidation flow reactors (OFRs) have recently become a popular alternative approach. OFRs typically have shorter residence times than chambers, which reduces wall contact. Also, ambient air can easily be oxidized in an OFR, while it is difficult and slow to perform such experiments in a large chamber (Tanaka et al., 2003). SOA yields from OH oxidation in OFRs for a variety of individual and mixed precursors have been reported and generally show that yields in OFRs are similar to chamber yields (Kang et al., 2007, 2011; Lambe et al., 2011, 2015; Li et al., 2013; Bruns et al., 2015). Properties

related to SOA elemental composition have also been investigated in OFRs (Massoli et al., 2010; Lambe et al., 2011, 2012, 2014; Saukko et al., 2012; Ortega et al., 2013, 2016). However, these studies were limited to laboratory-produced SOA from one or several precursor gases, often at very high concentrations. Several studies have reported on SOA formation from the OH oxidation of ambient air (Ortega et al., 2016; Palm et al., 2016) or emission sources (Cubison et al., 2011; Keller and Burtscher, 2012; Ortega et al., 2013; Tkacik et al., 2014; Bruns et al., 2015; Karjalainen et al., 2016; Timonen et al., 2016), but SOA from O_3 and NO_3 oxidation of ambient air or direct source emissions has not been studied using an OFR, to our knowledge.

In this study, we oxidized ambient pine forest air with either OH, O_3, or NO_3 in an OFR to investigate how much SOA can be formed from real ambient mixtures of largely biogenic SOA precursor gases, how the SOA precursor concentrations varied with time, and the properties of the SOA formed. The amount of SOA formed from each oxidant was compared to the amount predicted to form from oxidation of the measured ambient VOCs that entered the OFR. We investigated the elemental composition of the SOA that was formed as a function of the amount of oxidant exposure (oxidant concentration multiplied by residence time) in the OFR. The contribution of organic nitrate to SOA formation was also explored and compared to the results with ambient and chamber studies.

2 Experimental methods

2.1 BEACHON-RoMBAS field campaign

The OFR measurements presented here were conducted during July–August 2011 as part of the BEACHON-RoMBAS field campaign (Bio–hydro–atmosphere interactions of Energy, Aerosols, Carbon, H_2O, Organics and Nitrogen – Rocky Mountain Biogenic Aerosol Study; http://cires.colorado.edu/jimenez-group/wiki/index.php/BEACHON-RoMBAS). The research site was located in a ponderosa pine forest in a mountain valley at the Manitou Experimental Forest Observatory, near Woodland Park, Colorado (39.10° N, 105.10° W; 2370 m elevation). An overview of previous research at this site, including BEACHON-RoMBAS and prior campaigns, has been presented in detail by Ortega et al. (2014). Here we present a brief summary of research site details that are relevant to this analysis.

VOC concentrations at the site (quantified using proton-transfer-reaction time-of-flight mass spectrometry; PTR-TOF-MS) varied on a diurnal cycle, dominated by 2-methyl-3-buten-2-ol (MBO) during daytime and monoterpenes (MT) during nighttime. Fry et al. (2013) and Palm et al. (2016) show diurnal cycles of select biogenic and anthropogenic VOCs. VOC measurements from a July–September 2008

campaign at the same site have also been described in Kim et al. (2010). During BEACHON-RoMBAS, the concentration of MBO+isoprene in the forest canopy ranged from about 2 ppb during daytime to 0.4 ppb at nighttime (see Palm et al., 2016). The ratio of isoprene to MBO at this pine forest site was determined using NO^+ reagent ion chemical ionization mass spectrometry (Karl et al., 2012) and using GC-MS (Kaser et al., 2013) to be about 21 %, indicating the concentration of isoprene at this site was low (< 0.3 ppb). MT concentrations in the canopy spanned from 0.4 ppb during the day to 1.1 ppb at night, on average. The Manitou Experimental Forest Observatory site is mainly influenced by biogenic emissions, but it occasionally receives airflow from nearby urban areas (Denver metropolitan area and Colorado Springs, 75 and 35 km away from the site respectively), leading to moderate increases in NO_x (up to ~ 5 from ~ 2 ppbv), CO (up to ~ 140 from ~ 100 ppbv), and anthropogenic VOCs (e.g., benzene up to ~ 50 from ~ 20 pptv and toluene up to ~ 150 from ~ 50 pptv) during the late afternoon and evening (Fry et al., 2013; Ortega et al., 2014).

2.2 OFR methods

The OFR used in this study was the Potential Aerosol Mass (PAM) flow reactor (Kang et al., 2007, 2011). The PAM reactor is a cylindrical tube 45.7 cm long and 19.7 cm ID with a volume of approximately 13 L. This type of OFR has been used to study SOA formation and chemistry in a number of previous studies (e.g., Kang et al., 2007, 2011; Massoli et al., 2010; Lambe et al., 2012, 2015; Li et al., 2013; Ortega et al., 2013, 2016; Tkacik et al., 2014; Palm et al., 2016). During BEACHON-RoMBAS, ambient air was sampled through a 14 cm diameter opening on one end of the OFR (with the inlet plate removed to prevent loss of gases/particles on inlet surfaces) through a coarse-grid mesh screen coated with an inert silicon coating (Sulfinert by Silcotek, Bellefonte, PA). The OFR was located on top of the measurement trailer in order to sample ambient air directly without using an inlet. Therefore the temperature and RH inside the OFR were the same as ambient conditions, with the exception of minor heating from the UV lamps mounted inside the OH-OFR (up to ~ 2 °C heating at the highest lamp settings and ~ 0.5 °C at the settings producing the most SOA; Li et al., 2015). No heating occurred during O_3 or NO_3 modes. Thus RH within the OFR was the same or slightly lower than ambient, depending on the operating mode. The OFR was operated with a residence time in the range of 2–4 min. The residence time distribution in the OFR, modeled using FLUENT for the configuration used in this study (inlet plate removed), is shown in Fig. S1 in the Supplement. The modeled residence time distribution is much more homogeneous than has been measured for OFRs operated with an inlet plate (Lambe et al., 2011; Ortega et al., 2016). However, local winds can result in some variations that are not captured by the FLUENT model. The data were not screened for high local wind speeds. How-

ever, periods of high wind speeds were infrequent during the campaign, and the influence of local winds was likely tempered by the fact that the OFR was located within the canopy of the forest. Two OFRs were used simultaneously, with one dedicated to NO_3 oxidation while the other was used for either OH or O_3 oxidation. OH radicals were produced in situ inside the OFR using two different methods, referred to as OFR185 and OFR254 (named according to the wavelength of the highest energy UV light used to generate oxidants within the reactor). These methods have been described in detail previously and showed consistent results (Palm et al., 2016). All results of OH oxidation presented in this paper used the OFR185 method. The gas-phase HO_x/O_x chemistry and possible non-OH chemistry inside the OFR was investigated with kinetic modeling (Li et al., 2015; Peng et al., 2015, 2016). For the wide variety of compounds investigated in Peng et al. (2016), reactions with OH dominated over other possible reactions, including $O(^1D)$, $O(^3P)$, O_3, and photolysis at 185 or 254 nm, under the conditions of OH oxidation in the OFR during this campaign.

NO_3 radicals were generated by thermal decomposition of N_2O_5 ($N_2O_5 \rightarrow NO_2 + NO_3$), which was injected into the OFR from a cold trap held in a dry ice + isopropyl alcohol bath. The cold trap was held near $-60\,°C$ using a temperature controlled copper sleeve immersed in the $-78\,°C$ bath. A 10–100 sccm flow of zero air eluted N_2O_5 from the trap. This N_2O_5+zero air mixture was injected through an approximately 14 cm diameter ring of 1/8 in. Teflon tubing with pinholes around the ring mounted just inside the OFR entrance inside the mesh screen. N_2O_5 concentrations were adjusted by changing this flow rate from the N_2O_5 dry ice reservoir. The concentrations of N_2O_5 and NO_3 in both the injection flow and in the output of the OFR were measured using diode laser-based cavity ring-down spectroscopy (CRDS; Wagner et al., 2011). The concentration of NO_2 was measured in the output of the OFR using laser-induced fluorescence (Thornton et al., 2000). The experimental setup for the NO_3-OFR system is illustrated in Fig. S2 and discussed in Sect. S1 in the Supplement.

To estimate NO_3 concentrations and exposure in the OFR, the relevant chemistry was modeled using a chemical-kinetic plug-flow model, implemented in the KinSim chemical-kinetic integrator (version 3.10) using Igor Pro 6 (http://www.igorexchange.com/node/1333; Wavemetrics, Lake Oswego, OR, USA). A key output of this model was the integrated NO_3 exposure experienced by MT-containing air during the OFR residence time, calculated as the integral of NO_3 concentration over the OFR residence time (in units of molecules cm^{-3} s) and multiplied by the fraction of MT that was estimated to have been mixed with the N_2O_5 flow at each residence time, due to lack of mixing from the small flow rate (see Sect. S1 for more details of the unmixed fraction estimation and parameterization). NO_3 exposure was converted to an equivalent (eq.) atmospheric age by dividing by a typical site-specific nighttime ambient NO_3 concentration,

which has been estimated to be on the order of 1 ppt (Fry et al., 2013). This eq. age represents the amount of time the air would have to spend in the atmosphere with 1 ppt NO_3 to experience the same amount of NO_3 exposure as in the OFR. The unit of eq. age is a unit of exposure. When given in units of eq. days, it represents the number of 24 h periods that air would need to spend in an atmosphere containing the stated oxidant concentration in order to achieve the equivalent amount of exposure as in the OFR (which applies for OH and O_3 eq. ages as well). More details about the model can be found in Sect. S1.

The exposure metric for the NO_3-OFR is specific to the site in which it is measured. Fry et al. (2013) estimated the average nighttime NO_3 concentration at this site (approximately 1 pptv) from an average NO_3 production rate and lifetime of approximately 0.03 pptv s^{-1} and 25 s respectively. Other sites can have considerably different production rates for NO_3 and thus very different nighttime exposures. Remote forests, with nighttime NO_x below 50 pptv, could experience NO_3 production rates more than 10 times slower, while forests immediately downwind of urban areas could have NO_3 production rates more than 10 times faster (e.g., outflow from Houston, TX; Brown et al., 2013). Variability in NO_3 production rates and observed NO_3 levels is a common feature of recent field observations (Brown and Stutz, 2012). Estimated eq. NO_3 ages from this study are therefore shown simply for a common metric of comparison for all of the data during this study, interpretable in terms of the average chemistry occurring at the BEACHON site. Interpretation of measurements at other sites would need to be adjusted to local NO_3 concentrations.

To investigate SOA formation from O_3 oxidation, O_3 was produced external to the OFR by flowing pure dry O_2 gas across two low-pressure mercury UV lamps (BHK, Inc., model no. 82-9304-03). The O_2 was photolyzed by 185 nm light to produce $O(^3P)$, which further reacted with O_2 to produce O_3. This $O_2 + O_3$ mixture was injected at 0.5 lpm into the front of the OFR through four ports distributed evenly around and just inside the 14 cm opening. O_3 concentrations were cycled by adjusting the UV lamp intensity (i.e., photon flux) in the O_3 generation setup. O_3 was measured in the output of the OFR using a 2B Technologies model 205 Monitor. O_3 exposure was calculated by multiplying the measured O_3 concentration in the OFR output by the residence time of the OFR. Loss of injected O_3 to internal OFR walls was not investigated, so the exposure may be slightly underestimated by this method. O_3 exposure was converted to an eq. atmospheric age by dividing by a typical, site-specific, 24 h average, ambient O_3 concentration of 50 ppb. A schematic of the O_3-OFR system is also shown in Fig. S2.

2.3 Particle and gas measurements

Ambient and OFR-oxidized particles were measured with an Aerodyne high-resolution time-of-flight aerosol mass spec-

trometer (HR-ToF-AMS, referred to here as AMS; DeCarlo et al., 2006; Canagaratna et al., 2007) and a TSI 3936 scanning mobility particle sizer (SMPS). Details of these measurements have been described previously (Palm et al., 2016). Ambient VOC concentrations were quantified using a PTR-TOF-MS (Kaser et al., 2013). The OFR output was sampled by the PTR-TOF-MS during selected periods only (4–6, 9–10, and 22–23 August for NO_3 oxidation and 7–9 and 23–24 August for O_3 oxidation; see Palm et al. (2016) for details of sampling VOCs during OH oxidation). The particle mass measurements were corrected for particle losses to sampling line walls and at the small particle transmission limit of the AMS aerodynamic lens (combined 2 % correction; details of these corrections are the same as in Palm et al., 2016). To account for particle losses to internal OFR surfaces, the particle mass was corrected by the average ratio of ambient particle mass to the particle mass measured through each OFR in the absence of oxidant (1 % correction for the O_3 OFR, and 14 % for the NO_3 OFR due to a different sampling port with a higher wall surface-area-to-volume ratio).

A correction was also applied to account for any condensable oxidation products (referred to as low-volatility organic compounds; LVOCs) that were formed from gas-phase oxidation in the OFR but condensed on OFR or sampling line walls instead of condensing to form SOA. This is non-atmospheric behavior due to the short residence time in the OFR and the relatively small aerosol condensational sink in this study. A correction is needed because the dominant fate of such gases in the atmosphere will be condensation to form SOA (lifetime of ∼ minutes) rather than being lost to any environmental surfaces via dry or wet deposition (lifetime of ∼ hours to a day; Farmer and Cohen, 2008; Knote et al., 2015; Nguyen et al., 2015). This correction, referred to as the "LVOC fate correction", was first represented in a model developed in Palm et al. (2016); the full details of the model can be found there. Briefly, the model takes several inputs, including particle condensational sink, OFR residence time, and oxidant concentration. It produces the fractional fates of LVOCs with respect to condensation onto particles, condensation onto OFR walls, further oxidation to give non-condensable molecular fragmentation products, and condensation onto sampling line walls after exiting the back of the OFR. In Palm et al. (2016), the model was verified by quantitatively explaining SO_4 aerosol formation from OH oxidation of ambient SO_2.

The results of the LVOC fate model for the O_3-PAM and NO_3-PAM conditions in this study are shown in Fig. S3. The SOA formation values given in the subsequent analysis are corrected for LVOC fate by dividing the measured SOA formation by the fraction of LVOCs predicted to have condensed to form SOA in the OFR (an average correction of 0.4 µg m^{-3} for both O_3-PAM and NO_3-PAM). These corrected values refer to the amount of SOA that would form from any ambient precursors in the absence of OFR walls and the limited time for condensation within the OFR. LVOCs are

assumed not to be lost to fragmentation from excessive O_3 or NO_3 reactions in the gas phase prior to condensation due to lack of C = C bonds (which is different from the parameterization for OH reactions used in Palm et al., 2016). This assumption is reinforced by the fact that for the highest O_3 and NO_3 eq. ages achieved in this work, no net decrease of OA was observed when SOA-forming gases were not present (see Sect. 3.2.1 and Fig. 5). If fragmentation reactions in the gas phase (or from heterogeneous oxidation) were important for the range of eq. ages studied here, observations would show a net loss of OA at the highest eq. ages when SOA-forming gases (e.g., MT) were not present.

2.4 Modeling of SOA formation

In the analysis in Sect. 3.2.2, the amount of SOA formed by oxidation of ambient air by O_3 or NO_3 in the OFR is compared to the amount predicted to form. This predicted amount was estimated by applying SOA yields to the fraction of measured ambient MT and sesquiterpenes (SQT) concentrations that were predicted to react. Since the ambient VOC measurements were taken above the canopy at a height of 25 m, the concentrations were corrected to reflect in-canopy values that were ingested into the OFR, a technique which has been used previously (Kim et al., 2013; Wolfe et al., 2014; Palm et al., 2016). During this campaign, speciated MT and SQT measurements were not available. When predicting SOA formation in this analysis, we use previous measurements at the same site to approximate that MT consisted of an equal mix of α-pinene, β-pinene, and 3-carene and that SQT was solely isolongifolene (Kim et al., 2010). Numerous chamber studies have reported SOA yields of individual MT from O_3 oxidation (e.g., Ng et al., 2006; Pathak et al., 2007, 2008; Shilling et al., 2008; Zhao et al., 2015) and from NO_3 oxidation (Hallquist et al., 1999; Moldanova and Ljungström, 2000; Spittler et al., 2006; Fry et al., 2009, 2011, 2014; Boyd et al., 2015; Ng et al., 2017). SOA yields from SQT have also been reported for O_3 oxidation (Jaoui et al., 2003, 2013; Ng et al., 2006; Winterhalter et al., 2009; Chen et al., 2012; Tasoglou and Pandis, 2015) and NO_3 oxidation (Fry et al., 2014). In this analysis, the OA concentrations measured after O_3 or NO_3 oxidation ranged from 1 to 3 µg m^{-3}, with few exceptions. For simplicity with this relatively narrow range, the dependence of SOA yields on OA concentrations was not included. Instead, we applied representative SOA yields of 15 % for ozonolysis of α-pinene, β-pinene, and 3-carene and 30 % for ozonolysis of isolongifolene. For reaction with NO_3, SOA yields of 4, 33, 38, and 86 % were used for α-pinene, β-pinene, 3-carene, and isolongifolene (using β-caryophyllene as a proxy for all SQT; Fry et al., 2014; Kang et al., 2016; Ng et al., 2017). The rate constants used for reaction of α-pinene, β-pinene, 3-carene, and isolongifolene with O_3 and NO_3 were $k_{O_3} = 8.6 \times 10^{-17}$, 1.5×10^{-17}, 3.6×10^{-17}, and 1.1×10^{-17} cm^3 molec^{-1} s^{-1} and $k_{NO_3} = 6.1 \times 10^{-12}$,
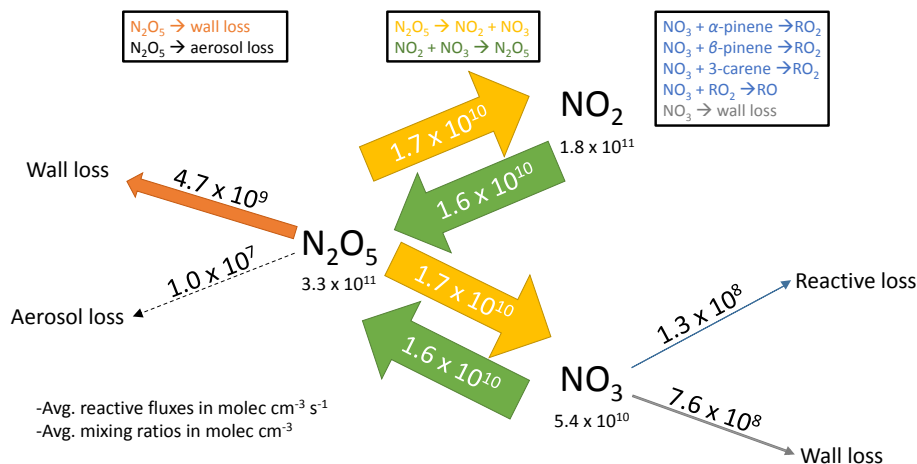
Figure 1. Typical average mixing ratios and reactive fluxes for the major reactions in the NO$_3$-OFR when injecting N$_2$O$_5$ to investigate SOA formation from NO$_3$ oxidation. These reactive fluxes resulted from running the model with inputs of 25 °C, 50 % RH, 50 ppb O$_3$, 2 ppb NO$_2$, 1.5 ppb NO$_3$, 50 ppb N$_2$O$_5$, 0.75 ppb total MT, and a rate constant for N$_2$O$_5$ uptake to aerosol surfaces of 3×10^{-5} s^{-1}. Reaction arrow widths are sized relative to their average reactive fluxes. Reactions that were included in the model (shown in Table S1 in the Supplement) but with smaller average rates are not shown here.

2.5×10^{-12}, 9.5×10^{-12}, and 3.9×10^{-12} cm^3 molec^{-1} s^{-1} respectively (Canosa-Mas et al., 1999; Atkinson and Arey, 2003; Richters et al., 2015).

3 Results and discussion

3.1 Modeled vs. measured NO$_3$ and O$_3$ exposures

One of the features of the OFR technique is the short residence time required for conducting high-time-resolution ambient measurements. Combined with the ability to rapidly change the amount of oxidant injected or produced in the OFR, this allows for a wide range of oxidation levels to be studied in a short amount of time (and thus with limited variation of ambient conditions). In this work, the oxidant concentration was changed every 20–30 min, covering a range from no added oxidant to maximum oxidation repeatedly in 2–3 h cycles. In order to interpret the results over the wide range of oxidant exposure, the amount of exposure must be quantified. In Palm et al. (2016), OH exposure was estimated using a model-derived equation (Li et al., 2015; Peng et al., 2015) and calibrated using PTR-TOF-MS measurements of VOC decay in the OFR. In this work, a simple box model was developed and compared with VOC decay measurements to estimate NO$_3$ and O$_3$ exposures in the OFR.

The set of reactions and rate constant parameters included in the modeling of NO$_3$ exposure are shown in Table S1. Figure 1 illustrates the most important mixing ratios and reactive fluxes in the OFR with injected N$_2$O$_5$ under typical conditions. Interconversion between N$_2$O$_5$ and NO$_2$+NO$_3$ was relatively rapid, which maintained the system near equilibrium at all times. Wall loss of N$_2$O$_5$ was estimated to be the

main loss of the injected nitrogen-containing species (84 %), while reaction of NO$_3$ with biogenic gases (2 %), NO$_3$ wall losses (14 %), and hydrolysis of N$_2$O$_5$ on particle surfaces (0.2 %) were minor loss pathways. Figure 2a–c compare the N$_2$O$_5$, NO$_2$, and NO$_3$ mixing ratios measured in the OFR output with those predicted by the model. The model is generally consistent with the measurements. The scatter in the measurements is thought to be due mainly to incomplete and/or variable mixing of the injected N$_2$O$_5$ flow into the sampled ambient air (see Sect. S1 for more details), with some contribution from measurement variability at low ambient MT concentrations. The critical output of this model for our application is the prediction of the fraction of MT reacted. Figure 2d shows that the model can reproduce the measured MT decay with an error (average absolute value of modeled minus measured fraction MT remaining) of 11 %, providing confirmation that using the model output NO$_3$ exposure in the subsequent analysis of aerosol mass yields from the OFR is justified. A similar analysis of SQT decay was not possible, because ambient SQT concentrations were too small to accurately measure fractional decays. Also, MBO did not react substantially with NO$_3$ in the OFR, consistent with the lifetime for reaction of NO$_3$ with MBO that is approximately 3 orders of magnitude slower than for reaction with MT (Atkinson and Arey, 2003). This is also representative of the atmosphere, where MBO will overwhelmingly react with OH or O$_3$ and not NO$_3$ (Atkinson and Arey, 2003).

Unlike NO$_3$ exposure, the estimation of O$_3$ exposure did not require a detailed chemical model since the O$_3$ system had no reservoir species analogous to N$_2$O$_5$. O$_3$ exposure was simply estimated as the measured O$_3$ concentration in the OFR output multiplied by residence time. To verify this estimate, the measured fraction of MT that reacted in the
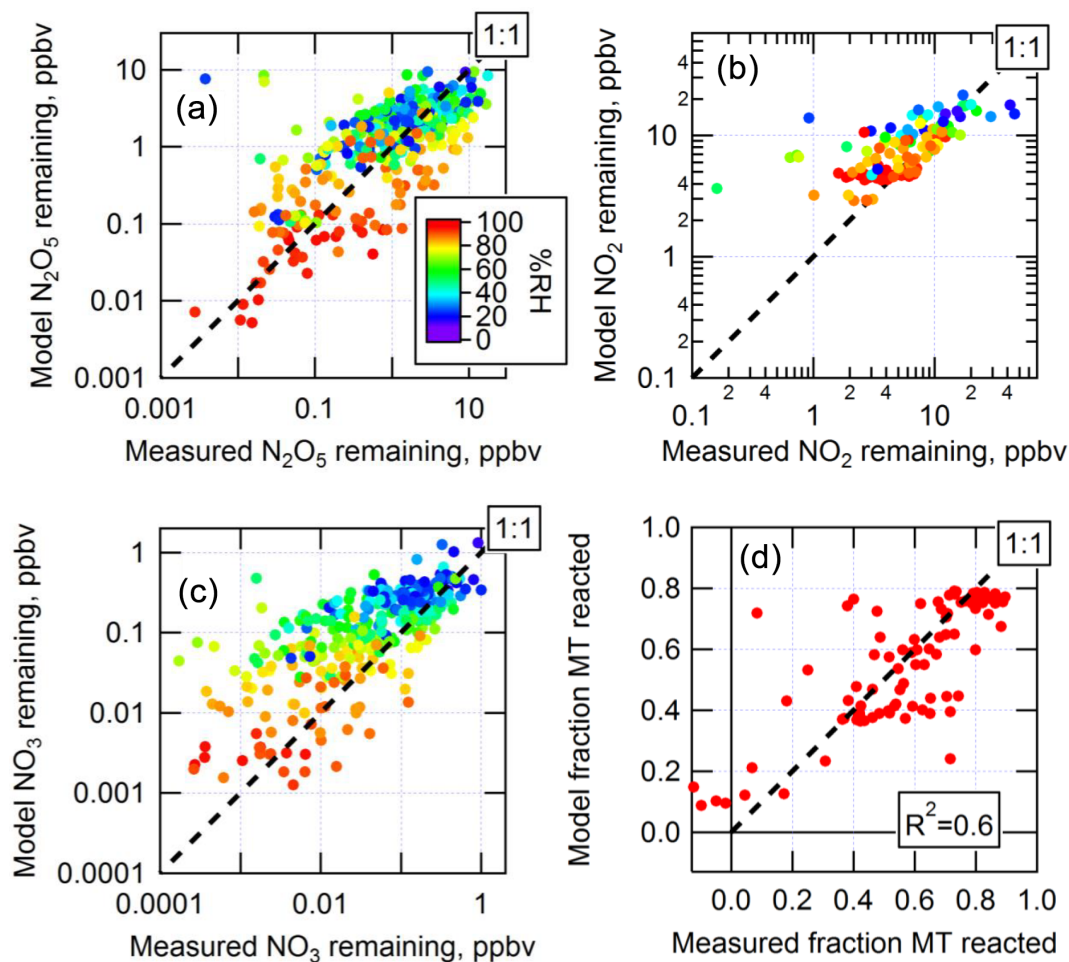
Figure 2. Modeled vs. measured **(a)** N_2O_5, **(b)** NO_2, **(c)** NO_3, and **(d)** fraction of ambient MT reacted with NO_3 in the output of the NO_3-OFR.
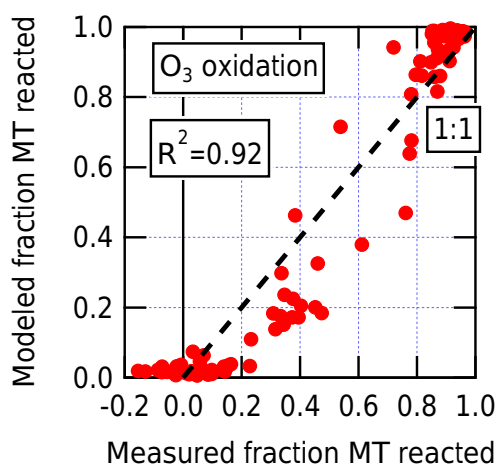

Figure 3. Modeled vs. measured fraction MT reacted by O_3 oxidation in the O_3-OFR.

OFR was compared in Fig. 3 to a model prediction calculated using a simple set of reactions of ozone with the three major MT species (Table S2). The model is consistent with measurements within an error of 9 % and shows that a parameterization for mixing of the O_3 flow into ambient air was not needed. In contrast to the slower 10–100 sccm flow of N_2O_5, the 0.5 lpm flow of O_2+O_3 appears to have been large enough relative to the total OFR flow rate to result in sufficiently complete mixing. This result suggests that a faster flow of N_2O_5 could be used in future NO_3 oxidation experiments to facilitate better mixing.

Time series examples of measured and modeled MT remaining after OFR oxidation are compared to ambient MT concentrations for both NO_3 and O_3 oxidation in Fig. 4. These examples illustrate the dynamic range from no MT reacted (i.e., when no oxidants were added to the ambient air) to nearly all MT reacted within the 2–3 h cycles for both oxidants. Further examples are shown for NO_3 oxidation in Fig. S6 and for O_3 oxidation in Fig. S7.
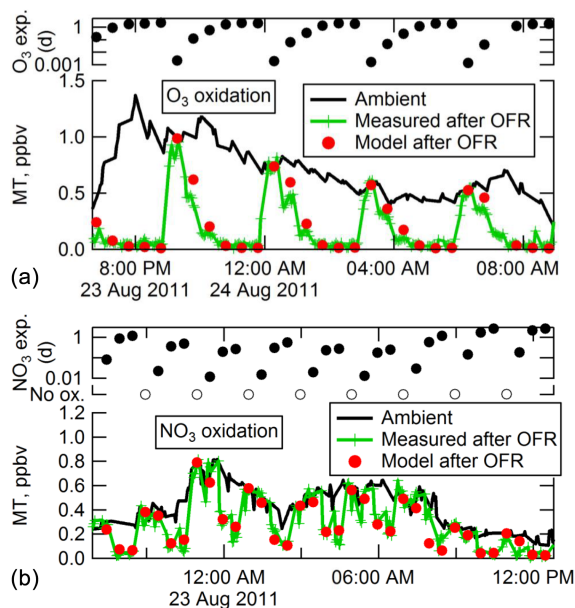
Figure 4. Ambient, measured remaining, and modeled remaining MT from O_3 oxidation on 23–24 August **(a)** and NO_3 oxidation on 22–23 August **(b)** in the OFR. Modeled O_3 and NO_3 exposures are also shown. The amount of oxidation was cycled from no added oxidant (no MT reacted) to maximum oxidation (most or all MT reacted) in repeated 2–3 h cycles.

3.2 SOA formed from oxidation of ambient air

3.2.1 OA enhancement vs. photochemical age

During BEACHON-RoMBAS, ambient air was oxidized by either OH, O_3, or NO_3 in order to study the amount and properties of SOA that could be formed from ambient precursors. In situ SOA formation from OH oxidation was the subject of a previous paper (Palm et al., 2016). Select results are reproduced here as a comparison to SOA formation from O_3 and NO_3 oxidation. Additional new analyses of the chemical composition of SOA formed from OH oxidation are also included along with O_3 and NO_3 oxidation in Sect. 3.3–3.4.

In Palm et al. (2016), SOA formation from OH oxidation in the OFR correlated with ambient MT concentrations (and implicitly with any other gases that correlated with MT, such as SQT and possibly terpene oxidation products). Here, Fig. 5 shows the OA enhancement observed after O_3 and NO_3 oxidation as a function of eq. age in the OFR. Similar to OH oxidation, little SOA formation was observed from O_3 or NO_3 oxidation when ambient MT concentrations were low, regardless of the amount of exposure. When MT concentrations were higher, increasing amounts of SOA were formed with increasing exposure. As seen in Fig. 5 (and in Fig. 6 below), lower eq. NO_3 ages were achieved when MT concentrations were higher, and higher eq. NO_3 ages were achieved when MT concentrations were lower. This was because the higher MT concentrations occurred during nighttime, when

lower ambient temperatures shifted the equilibrium towards N_2O_5 and away from $NO_2 + NO_3$ (from the injected N_2O_5), meaning lower NO_3 exposures were realized in the OFR.

Another way to examine the trends in OA enhancement is by separating the results into daytime and nighttime. Due to diurnal cycles in the emission rates (that are strong functions of temperature, and also light for some species), vertical mixing in the boundary layer, and changing rates of ambient oxidation, the concentration of MT (and other SOA precursors) in ambient air showed substantial diurnal cycles (Kim et al., 2010; Fry et al., 2013; Kaser et al., 2013). Ambient air was characterized by higher MBO+isoprene (with ambient OH and O_3 chemistry) during the day and higher MT+SQT (with ambient O_3 and NO_3 chemistry) during the night (Fry et al., 2013). Due to these changes, it might be expected that SOA formation in the OFR would also change diurnally.

OA enhancements vs. eq. age for OH, O_3, and NO_3 oxidation are shown together in Fig. 6, split between daytime (08:00–20:00 LT) and nighttime (20:00–08:00 LT). For all oxidants, more SOA formation was observed during nighttime. This is consistent with the general increase in MT and SQT (average of 1.1 and 0.04 ppbv in the canopy during nighttime and 0.4 and 0.03 ppbv during daytime respectively) and related precursor concentrations in the shallower nighttime boundary layer. This higher SOA formation during nighttime was not a result of larger temperature-dependent partitioning to the particle phase at lower nighttime temperatures, as evidenced by stable values of measured OA enhancement per unit ambient MT (the dominant measured SOA precursor) across the whole range of ambient temperatures (shown in Fig. S8). An exploration of the correlation between maximum SOA formation from each oxidant and all available ambient VOC concentrations is shown in Fig. S9, illustrating that MT are the best tracer of SOA production at this forest site. The maximum amount of SOA formed from OH oxidation was approximately 4 times more than from O_3 or NO_3 oxidation for both daytime and nighttime over the eq. ages covered in this work. If the gases that formed SOA from each oxidant were the same, then this would require the SOA yields from OH oxidation to be more than 4 times larger than from O_3 or NO_3 oxidation. The references for SOA yields from O_3 and NO_3 oxidation presented herein and for OH oxidation presented in Palm et al. (2016) show this is likely not the case. Instead, one possible explanation for this result could be that a large fraction of SOA-forming gases found in ambient air do not have C = C bonds (e.g., MT oxidation products such as pinonic acid). Such molecules would typically not react appreciably with O_3 or NO_3 over the range of eq. ages achieved in this work but will still react with OH and may lead to SOA formation. Future O_3 and NO_3 oxidation studies should include higher eq. age ranges in order to investigate whether additional SOA could be formed from ambient precursors at higher ages. This concept will be discussed further in Sect. 3.2.2.
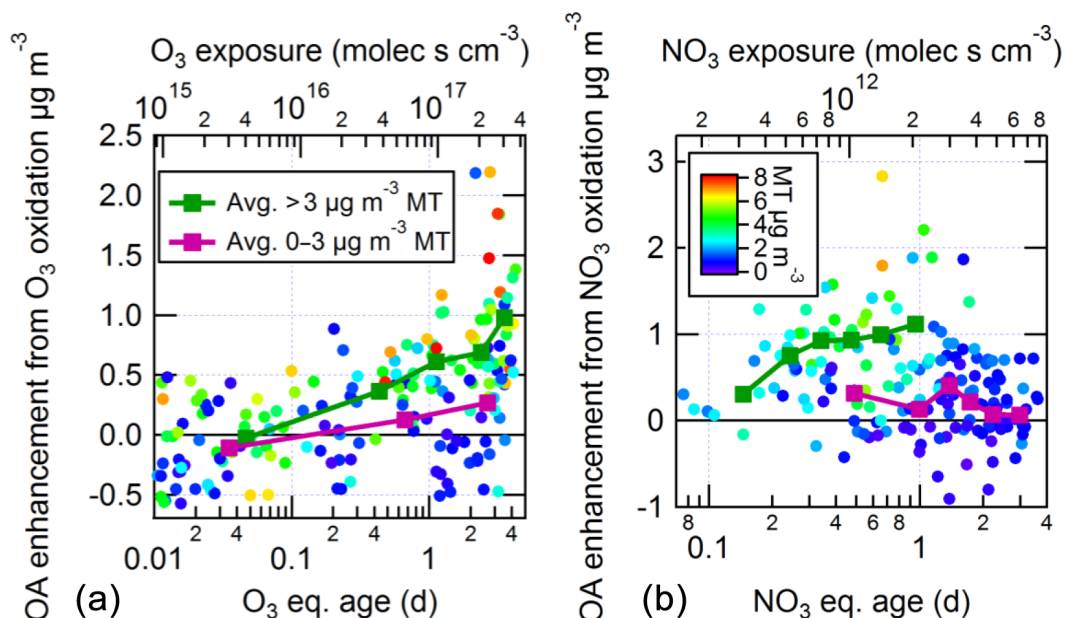
Figure 5. OA enhancement from oxidation of ambient air by O_3 **(a)** and NO_3 **(b)** as a function of oxidant exposure. Data are colored by ambient in-canopy MT concentrations and include the LVOC fate correction. Binned averages for times when ambient MT concentrations were either below or above $3\,\mu g\,m^{-3}$ (0.66 ppb) are also shown, illustrating the positive relationship between OA enhancement and MT concentrations at the higher oxidant concentrations.
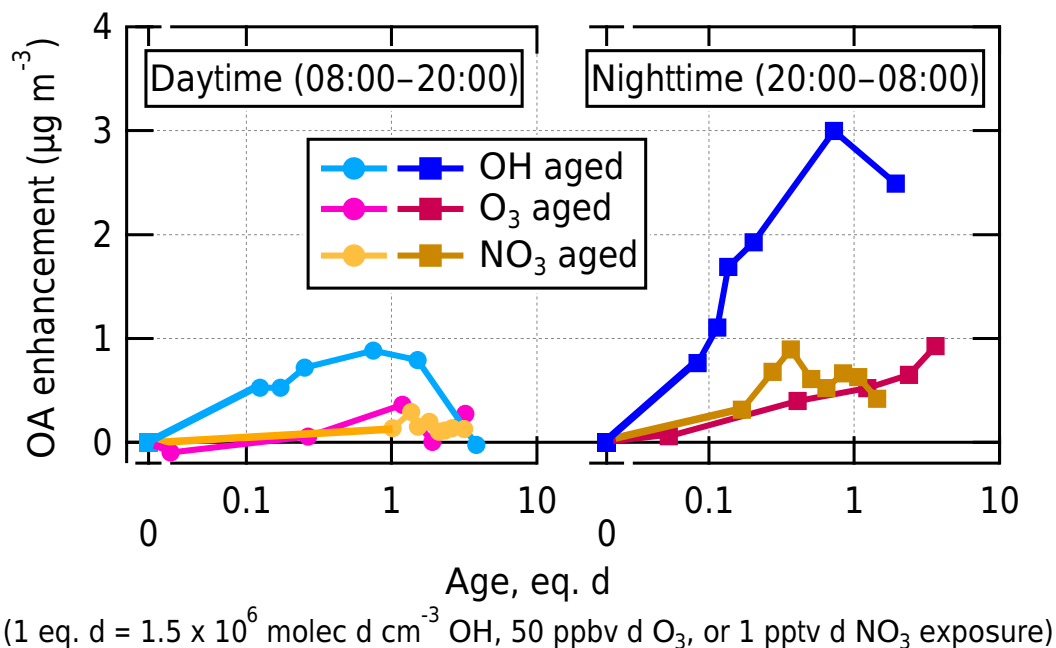

Figure 6. OA enhancement vs. age in eq. d for OH, O_3, and NO_3 oxidation, separated into daytime (08:00–20:00 LT) and nighttime (20:00–08:00 LT) data. All data are LVOC fate corrected. OH oxidation produced several-fold more OA enhancement than O_3 and NO_3 oxidation. OH-aged OA enhancement data (only for < 5 eq. d aging where the LVOC fate correction could be applied) are taken from Palm et al. (2016).

Whereas a net loss of OA was observed at > 10 eq. days of OH aging due to heterogeneous oxidation (shown in Fig. 7 of Palm et al., 2016), a similar net loss of OA at the highest eq. ages of O_3 and NO_3 oxidation was not observed. Since

the highest eq. ages for both O_3 and NO_3 oxidation were approximately 5 days, it is unclear whether O_3 or NO_3 heterogeneous oxidation would lead to net loss of ambient OA at substantially higher ages. Future experiments could be de-
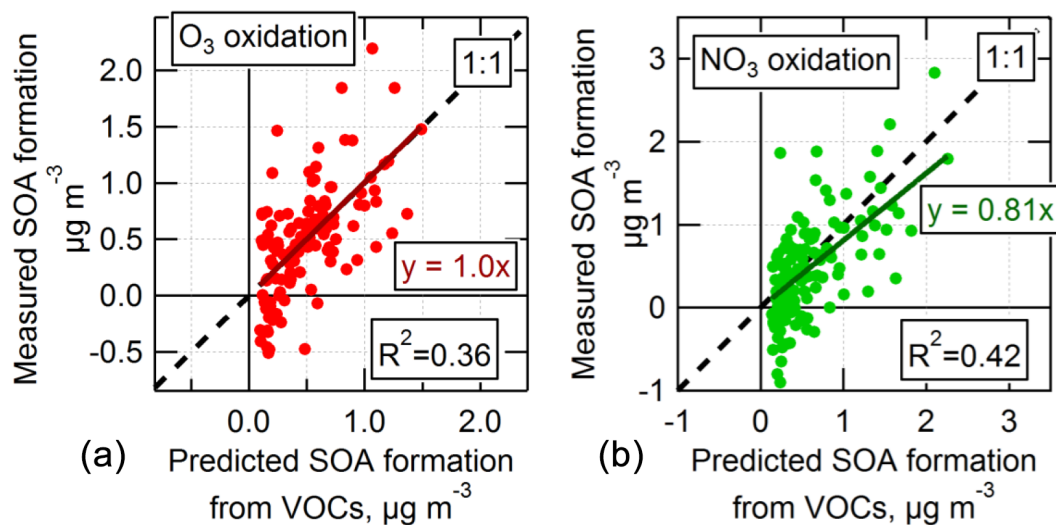
Figure 7. Measured vs. predicted SOA formation for O_3 and NO_3 oxidation in an OFR. The measured SOA formation includes the LVOC fate correction and includes all ages greater than 0.7 eq. d for O_3-PAM and greater than 0.3 eq. d for NO_3-PAM. Predicted SOA formation was estimated by applying published chamber SOA yields to the mass of VOCs predicted by the model to be oxidized in the OFR (see Sect. 2.3 for details).

signed to achieve higher ages in order to investigate this effect.

3.2.2 Measured vs. predicted OA enhancement

When ambient air is sampled into an OFR, any gases or particles present in that air are subject to oxidation. Measurement of the resultant SOA formation is a top-down measure of the total SOA formation potential of that air as a function of eq. age of oxidation. In other words, an OFR can be used to determine the relative concentrations of SOA-forming gases present in ambient air at any given time. To provide context to the measurements in the OFR, a bottom-up analysis can be carried out by applying laboratory SOA yields to the measured ambient SOA-forming gases that are entering the OFR.

The measured SOA formation after oxidation by O_3 and NO_3 is shown vs. the SOA predicted to form from measured precursor gases in Fig. 7. The measured SOA formation includes all ages greater than 0.7 eq. d for O_3-PAM and greater than 0.3 eq. d for NO_3-PAM, where most or all of the VOCs have reacted. For both oxidants, the data are scattered along the 1 : 1 line of equal measured and predicted SOA formation. This is in contrast to the analysis for OH oxidation in Palm et al. (2016), where a factor of 4.4 more SOA was formed from OH oxidation than could be explained by measured VOC precursors. As shown in that analysis, the additional SOA-forming gases in ambient air were likely S/IVOCs, where the SOA formation from S/IVOCs was 3.4 times larger than the source from VOCs. This conclusion was supported by unspeciated measurements of total S/IVOC concentrations (classified by volatility). SOA yields from S/IVOCs or any other sources are not required to ex-

plain SOA formation from O_3 or NO_3. This suggests that the majority of S/IVOCs in this ambient forest air generally did not contain C $=$ C bonds and therefore did not typically react with O_3 or NO_3 to produce SOA on atmospherically relevant timescales. This is consistent with expectations based on laboratory and ambient studies of MT and SQT oxidation products. Typical oxidation products include compounds such as pinic acid, pinonic acid, pinonaldehyde, caronaldehyde, and nopinone, none of which contain C $=$ C double bonds (e.g., Calogirou et al., 1999b; Yu et al., 1999; Lee et al., 2006). As an example, the reaction rates of pinonaldehyde with OH, O_3, and NO_3 are 3.9×10^{-11}, $< 2 \times 10^{-20}$, and $2.0 \times 10^{-14} \, \mathrm{cm^3 \, molec^{-1} \, s^{-1}}$ respectively (Atkinson et al., 2006). These rates correspond to eq. lifetimes of 4.7 h, > 579 days, and 29 days, respectively, showing that pinonaldehyde will typically only react with OH in the atmosphere or in the OFR under the conditions in this study.

While both the measured and predicted SOA formation shown in Fig. 7 are consistent with each other, two main caveats limit the strength of the conclusions that can be drawn from this particular study. First, the amount and dynamic range of SOA formed from O_3 and NO_3 oxidation were relatively small, as were the total ambient aerosol concentrations. This caused the SMPS+AMS measurement noise and variability to be larger relative to the total aerosol measurements than they would be for higher aerosol concentrations. Also, as only a small amount of new SOA was formed, the aerosol condensational sink remained relatively low for all measurements. According to the LVOC fate model, on average only 31 and 36 % of LVOCs condensed to form SOA during O_3 and NO_3 oxidation respectively (see Fig. S3). This required a correction of approximately a factor

of 3 to correct measured SOA formation to what would occur in normal atmospheric conditions.

3.3 H : C and O : C ratios of SOA formed from oxidation of ambient air

Analysis of ambient high-resolution AMS spectra can be used to estimate the elemental composition of OA (Aiken et al., 2008; Canagaratna et al., 2015). When SOA is formed in the OFR, the OA that is sampled in the OFR output is a sum of preexisting ambient OA and any SOA produced from oxidation. At sufficiently high eq. ages, the sampled OA will also include the effects of heterogeneous oxidation. The amount of O, C, and H atoms added by oxidation can be calculated by subtracting the ambient elemental concentrations from those measured after aging. The amounts of each element added by oxidation can be used to determine the O : C and H : C elemental ratios of the SOA that is formed in the OFR.

The amounts of O and H vs. C added from OH oxidation are shown in Fig. 8. Slopes were fit to the data with positive net addition of C in order to determine the O : C and H : C of the SOA formed for the eq. photochemical age ranges of 0.1–0.4 (avg. = 0.18) days, 0.4–1.5 (avg. = 0.9) days, 1.5–5 (avg. = 2.7) days, and 5–15 (avg. = 10) days. The elemental O : C (H : C) ratios of the SOA mass formed in those ranges were 0.55 (1.60), 0.84 (1.44), 1.13 (1.36), and 1.55 (1.22). For data with ages of longer than several eq. days, O was added coincident with loss of C (i.e., negative x intercept), which is likely due to heterogeneous oxidation leading to fragmentation/evaporation of preexisting OA. This conclusion is reinforced by the evidence that for eq. OH ages greater than several days, heterogeneous oxidation resulted in a net loss of C when ambient MT concentrations were low (Fig. S10), but not for lower eq. ages. Similarly, George and Abbatt (2010) suggested that the lifetime of ambient OA with respect to heterogeneous OH oxidation is approximately 2 to 3 days. Therefore, the change in amounts of O, C, and H after several eq. days of oxidation will be a mix of heterogeneous change to preexisting OA and addition of new SOA. These effects of heterogeneous oxidation (i.e., x and y intercepts) are likely to be approximately the same for all data within each given age range, meaning the slopes fitted above are independent of the heterogeneous processes and contain information about the elemental changes associated with the formation of varying amounts of SOA within each age range.

Analogous to Fig. 8, the amount of O and H vs. C added from O_3 and NO_3 oxidation is shown in Figs. 9–10. The SOA added from O_3 oxidation had O : C and H : C ratios of 0.50 and 1.61. The SOA added from NO_3 oxidation had O : C and H : C ratios of 0.39 and 1.60. This O : C value of 0.39 for NO_3 oxidation includes only the O atoms that were bound to the C backbone of the organic molecules and excludes the two O atoms that are bound only to N in the $-ONO_2$ (nitrate) functional group (Farmer et al., 2010). If all O atoms in the nitrate

functional group are included, the O : C of this added SOA mass was 0.44. Inclusion of only the carbon-bound oxygen of the nitrate functional group is more reflective of the carbon oxidation state and is also what is typically reported for AMS O : C measurements (since the organic $-NO_2$ moiety is measured in the AMS as total nitrate and typically not separated from inorganic nitrate).

Heterogeneous oxidation was not expected to be a factor for the O_3 and NO_3 ages used in this work. This assumption was reinforced by the fact that no net loss of C was observed for these amounts of oxidation, even when ambient MT concentrations (and OA enhancement) were low, as shown in Figs. S11–12. This assumption is also consistent with previous research on lifetimes of OA components with respect to O_3 and NO_3 heterogeneous oxidation. For instance, several aldehydes were found to have a relatively long lifetime equivalent to approximately 2–8 days for NO_3 heterogeneous oxidation when calculated using 1 pptv ambient NO_3 (Iannone et al., 2011). Ng et al. (2017) summarized that reactive uptake of NO_3 into particles is slow for most molecules, with the exception of unsaturated or aromatic molecules, which were unlikely to be major components of the ambient OA in this remote forest (Chan et al., 2016). Although the lifetime of pure oleic acid (which contains a C = C bond) particles with respect to heterogeneous O_3 oxidation can be as short as tens of minutes (Morris et al., 2002), lifetimes for oleic acid in atmospheric particle organic matrices can be tens of hours to days (Rogge et al., 1991; Ziemann, 2005). Furthermore, the uptake coefficients for O_3 to react with saturated molecules are typically 1–2 orders of magnitude slower than for unsaturated molecules (de Gouw and Lovejoy, 1998). In summary, this previous research suggests that heterogeneous oxidation by O_3 or NO_3 may be important at higher eq. ages, but not for those achieved in the present work.

To put the O : C and H : C values of the SOA formed in the OFR in perspective, Van Krevelen diagrams of H : C vs O : C ratios for OA measured after OH, O_3, and NO_3 oxidation are shown compared to concurrent measurements of ambient OA in Fig. 11a–c and summarized together in Fig. 11d. The effect of heterogeneous OH oxidation on preexisting aerosol is also shown as a line with a slope of -0.58. This line was fitted to the H : C vs. O : C of all OH-aged data where a net loss of C was observed (i.e., SOA formation was not observed and heterogeneous oxidation dominated). Generally speaking, less-oxidized ("fresh") OA will lie in the upper left portion of a Van Krevelen plot, with higher H : C values and lower O : C values. Conversely, more-oxidized ("aged") OA will move towards the lower right, with lower H : C values and higher O : C values (Heald et al., 2010; Ng et al., 2011). Shown in Fig. 11, the SOA formed from O_3, NO_3, and the lowest amount of OH aging (0.1–0.4 eq. days) was found at the upper left of the range occupied by ambient OA. As OH aging increased to higher ranges, the values of H : C decreased and the values of O : C increased, already moving beyond the local ambient range after 0.9 eq. days. At the higher ages, the
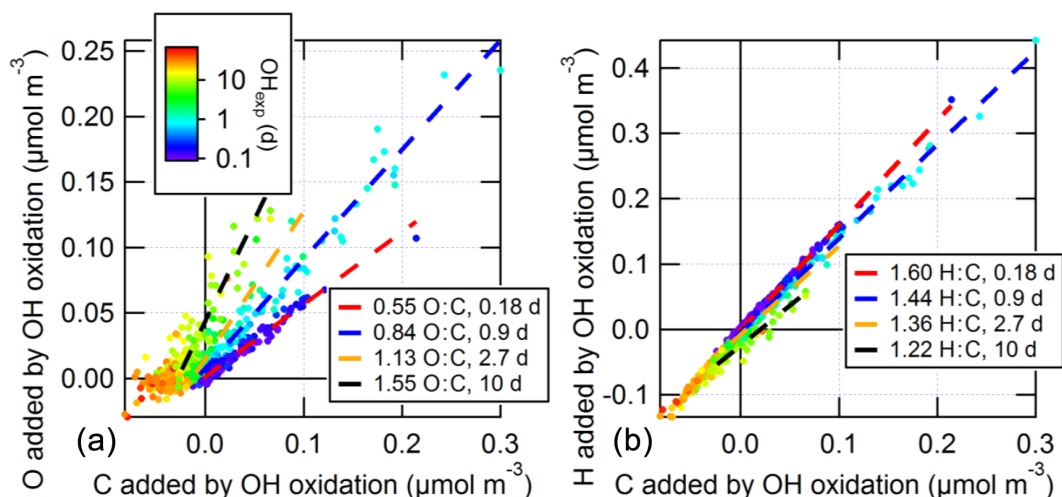
Figure 8. Scatter plots of µmol m^{-3} O and µmol m^{-3} H added per µmol m^{-3} C added from OH oxidation of ambient air in the OFR. Slopes are fit to the photochemical age ranges of 0.1–0.4 (avg. = 0.18) days, 0.4–1.5 (avg. = 0.9) days, 1.5–5 (avg. = 2.7) days, and 5–15 (avg. = 10) days, showing that the atomic O : C (H : C) ratios of the SOA mass formed in those ranges were 0.55 (1.60), 0.84 (1.44), 1.13 (1.36), and 1.55 (1.22) respectively. At higher ages, heterogeneous oxidation led to loss of C and H and little to no loss of O.
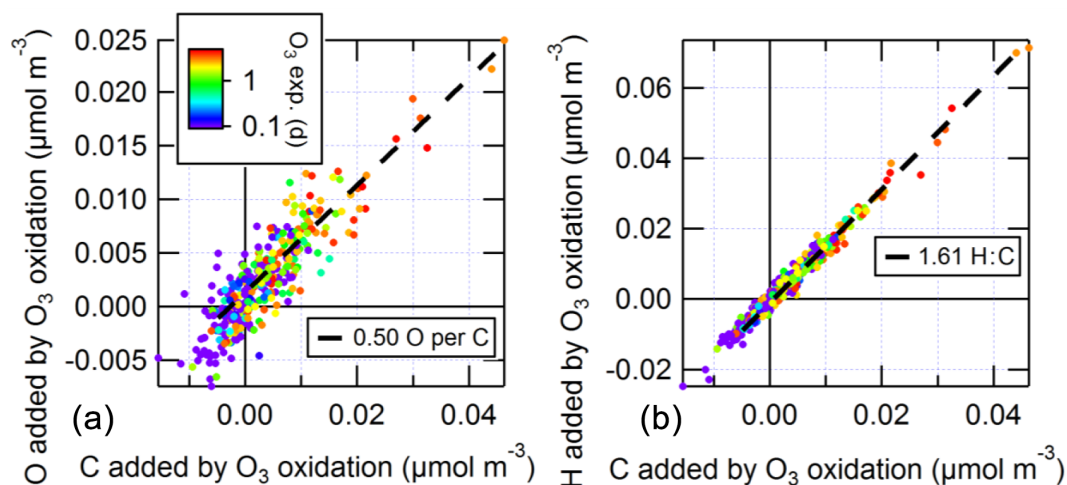
Figure 9. Scatter plots of µmol m^{-3} O and µmol m^{-3} H added per µmol m^{-3} C added from O$_3$ oxidation of ambient air in the OFR. Data are colored by eq. d of O$_3$ exposure. The slopes show that the atomic O : C (H : C) ratio of the SOA mass formed was 0.50 (1.61). The slopes did not change with increasing photochemical age.

H : C of the SOA formed lies at higher H : C values than those of the total OA measured after OH aging, which are closer to the trend of heterogeneous oxidation in the Van Krevelen space. This shows that SOA formed via gas-phase OH oxidation processes in an OFR has a higher H : C than the OA that results from heterogeneous oxidation, while both processes lead to similar increases in O : C. The net movement in the Van Krevelen space can be considered as starting at the ambient H : C and O : C and moving along two vectors: one vector along the heterogeneous oxidation line and another towards the H : C and O : C values of the new SOA formed in the gas phase, where the length of those two vectors is weighted by

the amount of OA resulting from each process. When little SOA is formed, the H : C and O : C measured after oxidation lie along the heterogeneous oxidation line. When high amounts of SOA are formed, the H : C and O : C after oxidation shift to higher H : C values, lying closer to the curve defined by the H : C and O : C of SOA mass added in the OFR at the different age ranges (see Fig. S13).

While these two vectors describe the possible oxidation processes in the OFR, there may be other vectors (e.g., from condensed-phase chemistry or reactive uptake) occurring in the atmosphere. As documented in Hu et al. (2016), SOA formation processes that require reactive uptake or within-
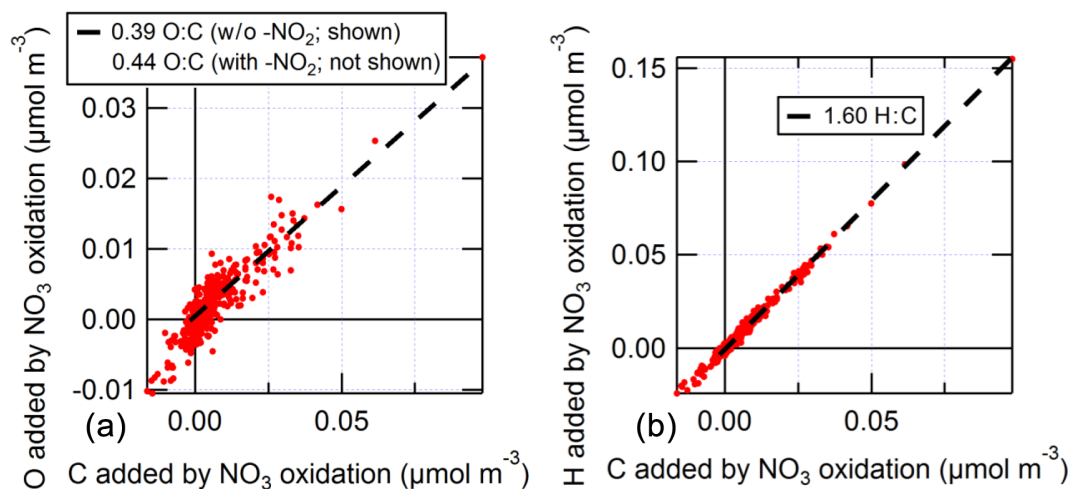
Figure 10. Scatter plots of μmol m^{-3} O and μmol m^{-3} H added per μmol m^{-3} C added from NO$_3$ oxidation of ambient air in the OFR. The amount of O added is shown without including the O from the $-$NO$_2$ group, since those O atoms do not affect the oxidation state of C. The slopes show that the atomic O : C(H : C) ratio of the SOA mass formed was 0.39 (1.60). The slopes did not change with increasing NO$_3$ exposure. Contrary to Figs. 8–9, data are not colored by NO$_3$ exposure. The ranges of NO$_3$ exposure achieved during daytime vs. nighttime were unequal (Figs. 5–6, S12), obscuring any trend of OA enhancement vs. eq. age.

particle non-radical chemistry (such as uptake of isoprene epoxydiols to form IEPOX-SOA) on timescales longer than the several minute residence time in the OFR are not captured with the OFR method used in this work. This is because the rate of reactive uptake and non-radical particle-phase chemistry do not speed up proportionally to increased OH and HO$_2$ (or O$_3$ or NO$_3$). However, to our knowledge the only precursor for which reactive uptake of epoxides has been shown to be a major pathway is isoprene, which was a very minor precursor at this site (Karl et al., 2012). The formation of epoxides during MBO oxidation has been proposed to play at role during BEACHON-RoMBAS (Zhang et al., 2012). However, recent results suggest that formation of epoxides during MBO oxidation is not important in the atmosphere (Knap et al., 2016). Thus, at this time it is not clear whether any important SOA-forming processes in this environment are missed by the OFR setup, and this question should be investigated in future studies.

The H : C of the least-oxidized SOA formed in the OFR from all oxidants was near 1.6. As discussed in Palm et al. (2016), SOA formation from OH oxidation in the OFR correlated with MT, and the S/IVOC sources of SOA may have been MT oxidation products or other related biogenic gases. Biogenic terpenes are composed of isoprene units, meaning they all have H : C of 1.6. Therefore, the SOA formed from the lowest eq. ages in the OFR was consistent with oxidation processes that add roughly 4–6 O atoms without removing net H atoms. Addition of $-$OH or $-$OOH functional groups after $-$H abstraction by OH radicals results in addition of O without loss of H and is consistent with the RO$_2$+HO$_2$ reaction conditions that are expected during OH oxidation in the OFR (Kroll and Seinfeld, 2008; Ortega et

al., 2016). OH can also add to a C$=$C bond, which could lead to addition of H atoms after oxidation. O$_3$ and NO$_3$ are expected to react with MT almost exclusively by addition to a C$=$C bond, which leads to addition of O without initial removal of H atoms (Atkinson and Arey, 2003). However, previous research has shown that many precursor gases, including aromatic molecules with initial H : C close to 1, can form SOA with H : C close to 1.6 (Chen et al., 2011; Chhabra et al., 2011; Canagaratna et al., 2015; Hildebrandt Ruiz et al., 2015). Therefore, H : C alone cannot provide direct evidence about the specific identities of precursor gases in ambient air. The SOA from O$_3$, NO$_3$, and 0.1–0.4 eq. days OH aging had H : C values similar to typical semivolatile oxidized organic aerosol (SV-OOA), while the H : C of SOA from 0.4 to 1.5 eq. days or longer OH aging resembled low-volatility oxidized organic aerosol (LV-OOA); these two types of SOA have been identified in ambient air at many locations (Jimenez et al., 2009; Canagaratna et al., 2015).

The relative timescales of oxidation and condensation in the OFR also need to be considered in order to properly interpret the H : C and O : C of the SOA mass formed in the OFR. In the atmosphere, once a molecule is oxidized to an LVOC that is able to condense onto a particle, lifetimes for condensation onto aerosols are on the order of several minutes (Farmer and Cohen, 2008; Knote et al., 2015; Nguyen et al., 2015). This is typically much shorter than the lifetimes for subsequent reaction with OH, O$_3$, or NO$_3$ of tens of minutes to several hours or longer, so condensation will likely occur prior to further oxidation. In OFR oxidation experiments, the lifetime for subsequent oxidation of LVOCs is shortened proportional to the increase in oxidant concentration. However,
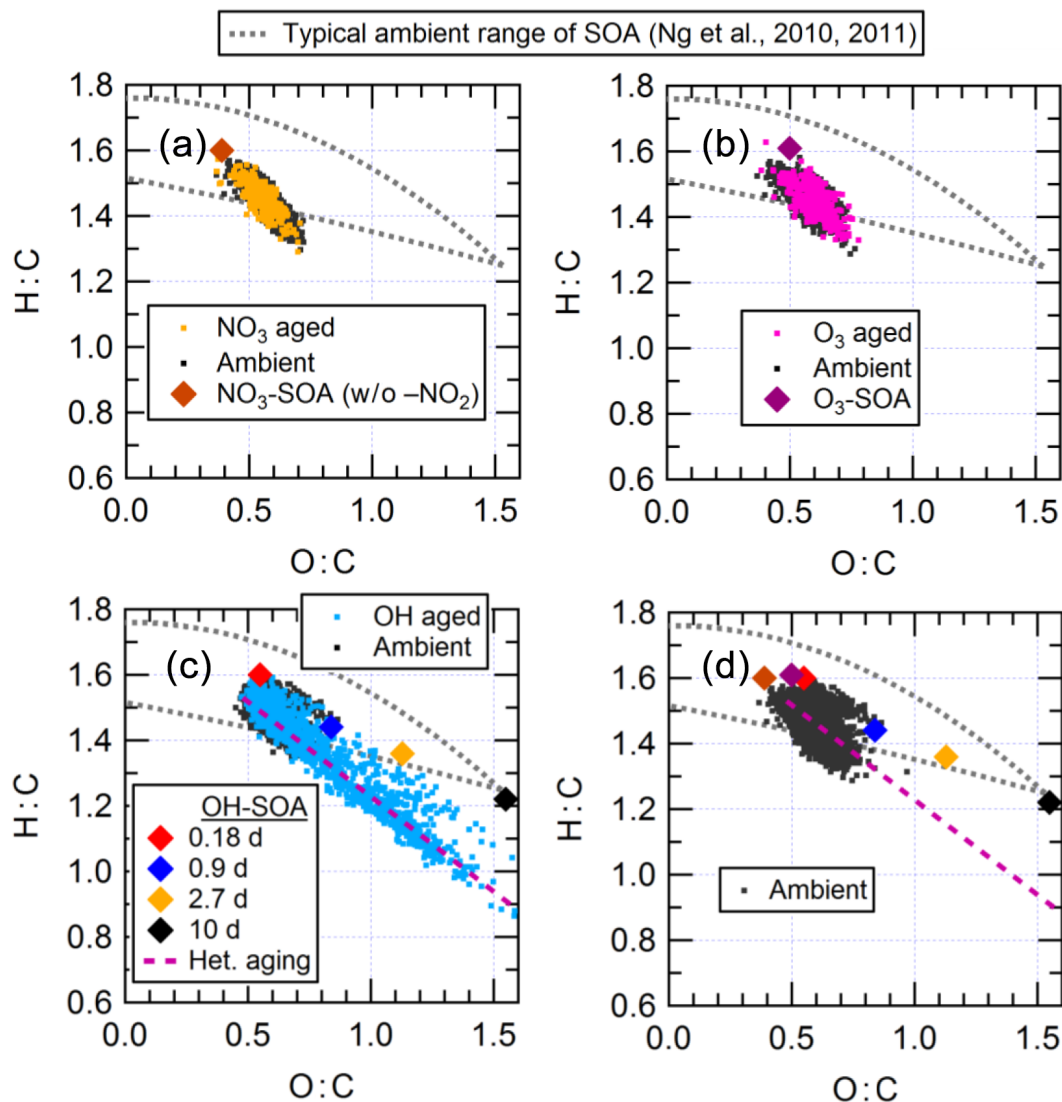
Figure 11. Van Krevelen diagrams of H : C vs. O : C ratios of OA after oxidation by **(a)** NO$_3$, **(b)** O$_3$, and **(c)** OH along with concurrent ambient ratios. The H : C and O : C ratios of the new SOA mass formed in the OFR (i.e., the slopes from Figs. 8–10) are shown for each oxidant (diamonds) and are summarized in **(d)** compared with all ambient measurements. For data where no net C addition was observed after OH oxidation, the slope along which heterogeneous OH oxidation transforms the ambient OA is shown (purple dashed line).

the condensation lifetime does not scale with oxidant concentration and remains roughly constant. At sufficiently high oxidant concentrations, LVOCs can be subjected to further oxidation steps that they would not be subjected to in the atmosphere prior to having a chance to condense to form SOA. To compare SOA formation in the OFR vs. ambient air, these relative timescales are considered here as a function of both oxidant type and amount of oxidant exposure.

The lowest range of OH aging for which O : C and H : C values were measured was 0.1–0.4 (avg. 0.18) eq. d, which is 2.4–9.6 (avg. 4.3) eq. *h* of oxidation. Typical terpenes have lifetimes for reaction with OH on the order of tens of minutes to several hours in the atmosphere (Atkinson and Arey,

2003), which is similar to this lowest eq. age range in the OFR. Typical terpene oxidation products have lifetimes ranging from 3.9 h (caronaldehyde; Alvarado et al., 1998) to 4.7 h (pinonaldehyde; Atkinson et al., 2006) to 11–13 h (nopinone; Atkinson and Aschmann, 1993; Calogirou et al., 1999a) to a computationally estimated 18–21 h (pinic and pinonic acid; Vereecken and Peeters, 2002). As a rough approximation, this suggests that the SOA formed in the OFR is likely a result of approximately one or at most a few oxidation steps occurring to the molecules that enter the OFR (which may have already experienced one or more oxidation steps in the atmosphere prior to entering the OFR). The aging in this range strikes a balance between achieving enough oxidation

to react all incoming precursors at least once while not reacting them an unrealistic number of times in the gas phase before allowing sufficient time for condensation. In the next age range of 0.4–1.5 (avg. 0.9) eq. d of OH aging, in which the maximum OA enhancement occurred, some primary precursors are likely starting to be oxidized multiple times inside the OFR prior to condensation, while some oxidation products will still be oxidized only ~ 1–2 times. The SOA formed in this range may represent SOA formed from multiple generations of chemistry. At higher ages in the OFR, the aerosol is likely mainly modified by heterogeneous oxidation, with a small contribution from condensation of highly oxidized products. This OA at the highest ages resembles ambient OA found in remote locations (Jimenez et al., 2009; Chen et al., 2015). Indeed, OFRs have previously been used to study heterogeneous oxidation processes (George et al., 2008; Smith et al., 2009).

For O_3 and NO_3 oxidation, the oxidants will react only with $C=C$ double-bond-containing gases. The major MT and SQT species at this field site all contain only a single $C=C$ bond (isoprene and minor MT and SQT species contain two). Subsequent reaction lifetimes of oxidation products with these oxidants will likely be longer than the lifetime for condensation onto particles. For example, the lifetimes for pinonaldehyde with respect to O_3 and NO_3 oxidation are > 579 days, and 29 days respectively (Atkinson et al., 2006). Therefore, we can approximate that multiple generations of oxidation are not dominant for SOA formation when investigating O_3 or NO_3 oxidation in the OFR at this site. This is consistent with previous chamber SOA formation experiments that suggested that first-generation oxidation products dominate SOA formation from O_3 oxidation of a variety of biogenic compounds with a single $C=C$ bond rather than products of later generations of oxidation (Ng et al., 2006). The SOA formed via O_3 or NO_3 oxidation in the OFR is likely formed from reaction with primary VOCs and a small subset of their reaction products that still contain $C=C$ bonds, such as the α-pinene oxidation product campholenic aldehyde (Kahnt et al., 2014). This SOA should be representative of typical atmospheric SOA formation processes.

3.4 Particulate organic nitrate (pRONO$_2$) formation from NO$_3$ oxidation of ambient air

In addition to estimating the elemental composition of OA, the AMS can also be used to estimate the amount of inorganic vs. organic nitrate in submicron aerosols (Farmer et al., 2010; Fry et al., 2013). The ratio of NO_2^+ to NO^+ fragment ions produced by thermal decomposition on the AMS vaporizer and electron impact ionization depends on the type of nitrate. NH_4NO_3 typically produces a ratio of approximately 0.3–1, while particulate organic nitrate (pRONO$_2$), in which the $-ONO_2$ functional group is covalently bonded to the carbon backbone (R) through an oxygen atom, typically produces a ratio ~ 2–3 times lower (Fry et al., 2009;

Bruns et al., 2010; Farmer et al., 2010; Liu et al., 2012; Day et al., 2017). The measured NO_2^+ to NO^+ ratio is a linear combination of these two chemical components. Using this principle, the NO_3 measured by the AMS was split into the estimated fractions of NH_4NO_3 and pRONO$_2$ according to the method described in Fry et al. (2013). For the instrument in this work, ratios of 0.3 and 0.13 were used for the NO_2^+ to NO^+ ratios of NH_4NO_3 and pRONO$_2$ respectively (Fry et al., 2013).

A two-night example of both ambient and NO_3-radical aged aerosol on 20–22 August is shown in Fig. 12. In ambient air, the majority of NO_3 aerosol was organic. After oxidation in the OFR, different behavior was seen on the two nights shown. On the first night, mainly inorganic nitrate was produced, as evidenced by the higher NO_2^+ to NO^+ ratio, the formation of NH_4 aerosol, and the relatively small amount of SOA formed. On the second night, pRONO$_2$ was produced, as evidenced by the lower NO_2^+ / NO^+ ratio, a lack of NH_4 aerosol formation, and substantial SOA formation. The organic nitrate formation and SOA formation also roughly tracked the ambient MT concentrations.

These two distinct behaviors in the NO_3-OFR were likely controlled by ambient RH. There was a competition between thermal dissociation of injected N_2O_5 to produce NO_3+NO_2 (favored at high temperatures and low RH) and the hydrolysis of N_2O_5 on wetted OFR walls to produce HNO_3 (favored at low temperatures and high RH). When hydrolysis occurred rapidly, there was a sharp decrease in N_2O_5 concentrations. The NO_3 radical concentrations were also greatly reduced, and thus fewer NO_3 radicals were available to react with ambient gases (e.g., MT) to produce pRONO2. HNO_3 reacted with NH_3 in ambient air or evaporating from OFR surfaces to produce NH_4NO_3. The results shown in Fig. 12 illustrate this behavior, with NO_3 radical exposure being reduced while NH_4NO_3 was produced during the first night. Despite the presence of similar MT concentrations on both nights, little SOA was produced on the first night. Future applications could include heating of the OFR slightly above ambient temperatures in order to prevent hydrolysis of N_2O_5 on the OFR walls. Inhibiting NH_4NO_3 formation artifacts would be especially critical for data interpretation if measuring aerosol enhancements with only non-chemical instruments such as an SMPS.

Despite this complex chemistry, information about the chemical composition of pRONO$_2$ formed from real atmospheric precursors can still be derived from times when conditions favored pRONO$_2$ formation. Shown in Fig. 13 is the mass of organic $-ONO_2$ added vs. SOA added from oxidation by each of the three oxidants. Substantial formation of pRONO$_2$ was observed only for NO_3 radical oxidation, and not for O_3 or OH oxidation. This was expected, since ambient NO_x concentrations were generally low (0.5–4 ppb; Ortega et al., 2014), and the NO_3 oxidation experiment was the only one with an added source of reactive nitrogen. The slopes of Fig. 13 represent the ratio of $-ONO_2$ to the rest
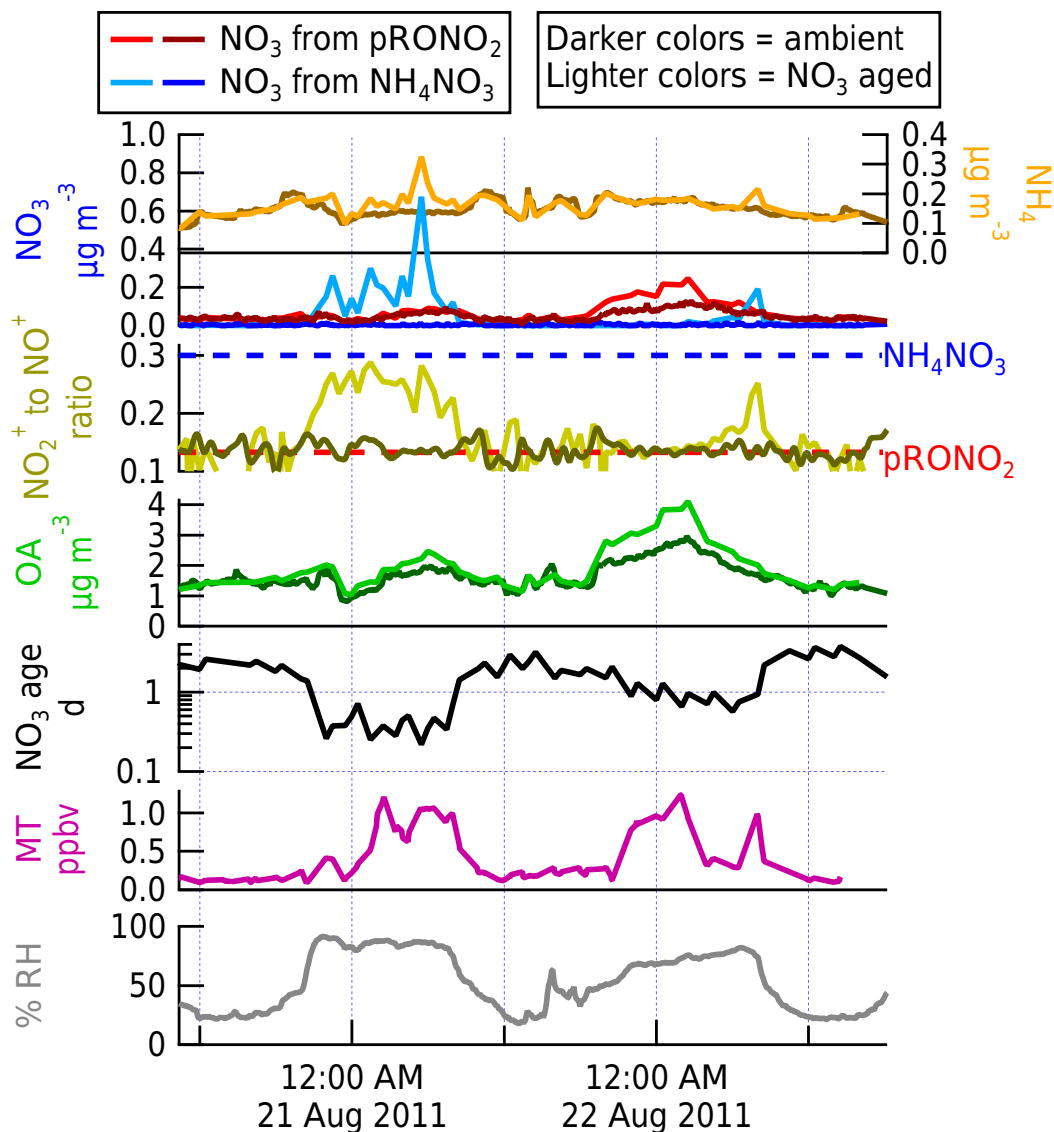
Figure 12. Example time series of OA, NH_4, and NO_3 (split into $pRONO_2$ and NH_4NO_3) aerosol measurements after NO_3 oxidation in the OFR, compared to ambient aerosol, NO_2^+ to NO^+ ratio, model-derived eq. age of NO_3 oxidation, MT concentration, and RH measurements. Production of both NH_4NO_3 and $pRONO_2$ was observed at different times, which appears to depend on changes in experimental conditions.

of the organic molecules in $pRONO_2$. In this study, the slope after NO_3 radical oxidation was 0.10, which is similar to the range of 0.1–0.18 found in previous chamber studies of NO_3 oxidation of terpenes (Fry et al., 2009, 2011; Boyd et al., 2015). To put this in context, if every SOA molecule formed in the OFR contained a single $-ONO_2$ group (with its mass of 62 g mol^{-1}), then the molecular mass of the full $pRONO_2$ molecules would be an average of 620 g mol^{-1} (giving the slope of 62 g mol^{-1}/620 g mol^{-1} = 0.10 in Fig. 13). Alternatively, if all molecules are assumed to have a mass of 200 or 300 g mol^{-1}, then 32 or 48 % of the molecules, respectively, would contain a $-ONO_2$ functional group (assuming no molecules contain more than one $-ONO_2$ group). Again,

this result is roughly consistent with previous research. For the fraction of OA composed of $pRONO_2$ in $NO_3 + \beta$-pinene SOA, Fry et al. (2009) estimated 32–41 % (assuming an average molecular weight of 215–231 g mol^{-1}), Fry et al. (2014) estimated 56 % (assuming 214 g mol^{-1}), and Boyd et al. (2015) estimated 45–68 % (assuming 200–300 g mol^{-1}).

4 Conclusions

In situ SOA formation from ambient pine forest air after oxidation by OH, O_3, or NO_3 radicals was measured using an OFR for the first time. SOA formation from these real am-
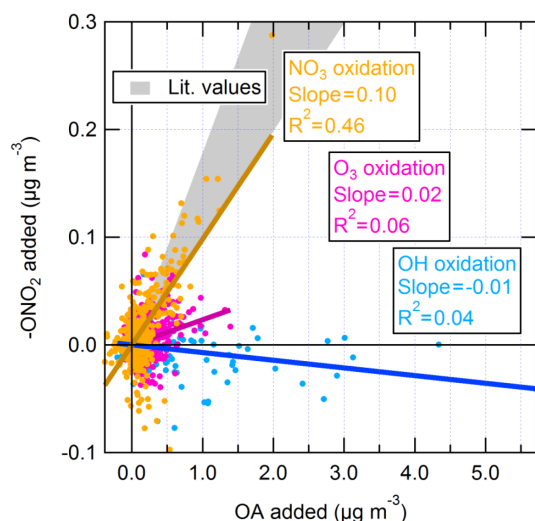
Figure 13. Organic $-ONO_2$ mass added vs. OA added from OH, O_3, and NO_3 oxidation in an OFR. No $pRONO_2$ formation was observed (or expected) from OH or O_3 oxidation under the experimental conditions. The slope of 0.10 from NO_3 oxidation is consistent with previous chamber measurements (shown in grey), which range from approximately 0.1 to 0.18 (Fry et al., 2009, 2011; Boyd et al., 2015).

bient mixes of aerosol and SOA precursors was measured semi-continuously, capturing diurnal and daily changes in the relative ambient concentrations of SOA precursor gases. In general, more SOA was formed from the precursors present in nighttime air than in daytime air for all three oxidants. At all times of day, OH oxidation produced approximately 4 times more SOA than O_3 or NO_3 oxidation. The O : C and H : C ratios of the SOA formed by O_3, NO_3, and several eq. hours of OH oxidation were similar to the oxidation levels of ambient OA.

The OFR is a tool that can be used to measure the total SOA formation potential of ambient air at any given time and how that potential changes with time, whether or not the SOA precursor gases are measured and/or speciated. As discussed in Palm et al. (2016), ambient VOC concentrations alone could not explain the amount of SOA formed in the OFR by OH oxidation. Instead, SOA was likely being formed from S/IVOCs that entered the OFR. In contrast, the quantity of measured VOCs was sufficient to explain the amount of SOA formed from O_3 and NO_3 oxidation; closure between measured and predicted SOA formation in an OFR was achieved. In other words, O_3 and NO_3 oxidation of the ambient S/IVOCs does not appear to produce appreciable amounts of SOA. This suggests that the ambient S/IVOCs tend not to have double bonds.

While this work does not investigate the source of the S/IVOCs, one possibility is that they are oxidation products of primary VOCs (e.g., MT or SQT). The primary VOCs could be emitted upwind of the site, and by the time the

molecule enters the OFR the double bond(s) will have reacted, leaving an oxidation product that reacts further with OH but not O_3 or NO_3. If the lifetime for further reaction of these oxidation products is slower than the lifetime for the double-bond-containing primary emissions, then the oxidation products will build up in the atmosphere. Under this hypothesis, such S/IVOC compounds are not new or unexpected sources of SOA. In most regional and global models, they would already be implicitly accounted for, by tracking the emissions of the primary VOCs which have corresponding overall SOA yields. In this work, we consider only the primary VOCs that are measured to be entering the OFR, not the integrated sum of upwind emissions that were emitted into the air that eventually entering the OFR after some degree of ambient photochemical processing. SOA formation in the OFR takes a snapshot of the atmosphere, which consists of a mix of primary emissions and their oxidation products at various stages of oxidative progress. For this study, those snapshots demonstrate that for OH oxidation only approximately a quarter of the SOA-forming gases are in the form of primary VOC, while for O_3 and NO_3 oxidation almost all are in the form of primary VOC. It also suggests that for these precursor mixtures, multi-generational chemistry plays a major role in the overall amount of SOA formed from OH oxidation (and much less so for O_3 and NO_3).

If these SOA-forming S/IVOCs do not react with ambient O_3 or NO_3, they will build up in the atmosphere during the night when OH is absent. When the sun rises and OH is produced, a sudden burst of SOA formation might be expected. However, this coincides with dilution of gases and particles due to convective vertical mixing, potentially offsetting such new SOA formation and making it difficult to observe it without detailed chemical and boundary layer dynamics measurements and/or modeling. These OFR measurements and analysis elucidate the presence and properties of S/IVOCs in the atmosphere and highlight the need for more measurements and modeling of such gases in order to better understand ambient SOA formation. This work also demonstrates the utility of the OFR as a tool for studying SOA formation from all three major atmospheric oxidants.

The Supplement related to this article is available online at doi:10.5194/acp-17-5331-2017-supplement.

References

Aiken, A. C., DeCarlo, P. F., Kroll, J. H., Worsnop, D. R., Huffman, J. A., Docherty, K. S., Ulbrich, I. M., Mohr, C., Kimmel, J. R., Sueper, D., Sun, Y., Zhang, Q., Trimborn, A., Northway, M., Ziemann, P. J., Canagaratna, M. R., Onasch, T. B., Alfarra, M. R., Prevot, A. S. H., Dommen, J., Duplissy, J., Metzger, A., Baltensperger, U., and Jimenez, J. L.: O/C and OM/OC Ratios of Primary, Secondary, and Ambient Organic Aerosols with High-Resolution Time-of-Flight Aerosol Mass Spectrometry, Environ. Sci. Technol., 42, 4478–4485, doi:10.1021/es703009q, 2008.

Alvarado, A., Arey, J., and Atkinson, R.: Kinetics of the Gas-Phase Reactions of OH and NO_3 Radicals and O_3 with the Monoterpene Reaction Products Pinonaldehyde, Caronaldehyde, and Sabinaketone, J. Atmos. Chem., 31, 281–297, doi:10.1023/A:1006010915971, 1998.

Atkinson, R.: Gas-Phase Tropospheric Chemistry of Volatile Organic Compounds: 1. Alkanes and Alkenes, J. Phys. Chem. Ref. Data, 26, 215–290, doi:10.1063/1.556012, 1997.

Atkinson, R. and Arey, J.: Gas-phase tropospheric chemistry of biogenic volatile organic compounds: a review, Atmos. Environ., 37, 197–219, doi:10.1016/S1352-2310(03)00391-1, 2003.

Atkinson, R. and Aschmann, S. M.: Atmospheric chemistry of the monoterpene reaction products nopinone, camphenilone, and 4-acetyl-1-methylcyclohexene, J. Atmos. Chem., 16, 337–348, doi:10.1007/BF01032629, 1993.

Atkinson, R., Winer, A. M., and Pitts Jr., J.: Rate constants for the gas-phase reactions of O_3 with the natural hydrocarbons isoprene and α and β-pinene, Atmos. Environ., 16, 1017–1020, 1982.

Atkinson, R., Baulch, D. L., Cox, R. A., Crowley, J. N., Hampson, R. F., Hynes, R. G., Jenkin, M. E., Rossi, M. J., Troe, J., and IUPAC Subcommittee: Evaluated kinetic and photochemical data for atmospheric chemistry: Volume II – gas phase reactions of organic species, Atmos. Chem. Phys., 6, 3625–4055, doi:10.5194/acp-6-3625-2006, 2006.

Bertram, A. K., Martin, S. T., Hanna, S. J., Smith, M. L., Bodsworth, A., Chen, Q., Kuwata, M., Liu, A., You, Y., and Zorn, S. R.: Predicting the relative humidities of liquid-liquid phase separation, efflorescence, and deliquescence of mixed particles of ammonium sulfate, organic material, and water using the organic-to-sulfate mass ratio of the particle and the oxygen-to-carbon elemental ratio of the organic component, Atmos. Chem. Phys., 11, 10995–11006, doi:10.5194/acp-11-10995-2011, 2011.

Boyd, C. M., Sanchez, J., Xu, L., Eugene, A. J., Nah, T., Tuet, W. Y., Guzman, M. I., and Ng, N. L.: Secondary organic aerosol formation from the β-pinene+NO_3 system: effect of humidity and peroxy radical fate, Atmos. Chem. Phys., 15, 7497–7522, doi:10.5194/acp-15-7497-2015, 2015.

Brown, S. S. and Stutz, J.: Nighttime radical observations and chemistry, Chem. Soc. Rev., 41, 6405, doi:10.1039/c2cs35181a, 2012.

Brown, S. S., Dubé, W. P., Bahreini, R., Middlebrook, A. M., Brock, C. A., Warneke, C., de Gouw, J. A., Washenfelder, R. A., Atlas, E., Peischl, J., Ryerson, T. B., Holloway, J. S., Schwarz, J. P., Spackman, R., Trainer, M., Parrish, D. D., Fehshenfeld, F. C., and Ravishankara, A. R.: Biogenic VOC oxidation and organic aerosol formation in an urban nocturnal boundary layer: aircraft vertical profiles in Houston, TX, Atmos. Chem. Phys., 13, 11317–11337, doi:10.5194/acp-13-11317-2013, 2013.

Bruns, E. A., Perraud, V., Zelenyuk, A., Ezell, M. J., Johnson, S. N., Yu, Y., Imre, D., Finlayson-Pitts, B. J., Alexander, M. L., Bruns, A. E., Perraud, V., Zelenyuk, A., Ezell, M. J., Johnson, S. N., Yu, Y., Imre, D., Finlayson-Pitts, B. J., and Alexander, M. L.: Comparison of FTIR and particle mass spectrometry for the measurement of particulate organic nitrates, Environ. Sci. Technol., 44, 1056–61, doi:10.1021/es9029864, 2010.

Bruns, E. A., El Haddad, I., Keller, A., Klein, F., Kumar, N. K., Pieber, S. M., Corbin, J. C., Slowik, J. G., Brune, W. H., Baltensperger, U., and Prévôt, A. S. H.: Inter-comparison of laboratory smog chamber and flow reactor systems on organic aerosol yield and composition, Atmos. Meas. Tech., 8, 2315–2332, doi:10.5194/amt-8-2315-2015, 2015.

Calogirou, A., Jensen, N. R., Nielsen, C. J., Kotzias, D., and Hjorth, J.: Gas-Phase Reactions of Nopinone, 3-Isopropenyl-6-oxo-heptanal, and 5-Methyl-5-vinyltetrahydrofuran-2-ol with OH, NO_3, and Ozone, Environ. Sci. Technol., 33, 453–460, doi:10.1021/es980530j, 1999a.

Calogirou, A., Larsen, B. R., and Kotzias, D.: Gas-phase terpene oxidation products: a review, Atmos. Environ., 33, 1423–1439, doi:10.1016/S1352-2310(98)00277-5, 1999b.

Calvert, J. G., Atkinson, R., Becker, K. H., Kamens, R. M., Seinfeld, J. H., Wallington, T. H., and Yarwood, G.: The Mechanisms of Atmospheric Oxidation of the Aromatic Hydrocarbons, Oxford University Press, New York, USA, 2002.

Canagaratna, M. R., Jayne, J. T., Jimenez, J. L., Allan, J. D., Al-farra, M. R., Zhang, Q., Onasch, T. B., Drewnick, F., Coe, H., Middlebrook, A., Delia, A., Williams, L. R., Trimborn, A. M., Northway, M. J., DeCarlo, P. F., Kolb, C. E., Davidovits, P., and Worsnop, D. R.: Chemical and microphysical characterization of ambient aerosols with the aerodyne aerosol mass spectrometer, Mass Spectrom. Rev., 26, 185–222, doi:10.1002/mas.20115, 2007.

Canagaratna, M. R., Jimenez, J. L., Kroll, J. H., Chen, Q., Kessler, S. H., Massoli, P., Hildebrandt Ruiz, L., Fortner, E., Williams, L. R., Wilson, K. R., Surratt, J. D., Donahue, N. M., Jayne, J. T., and Worsnop, D. R.: Elemental ratio measurements of organic compounds using aerosol mass spectrometry: characterization, improved calibration, and implications, Atmos. Chem. Phys., 15, 253–272, doi:10.5194/acp-15-253-2015, 2015.

Canosa-Mas, C. E., King, M. D., Scarr, P. J., Thompson, K. C., and Wayne, R. P.: An experimental study of the gas-phase reactions of the NO_3 radical with three sesquiterpenes: isolongifolene, al-loisolongifolene, and α-neoclovene, Phys. Chem. Chem. Phys., 1, 2929–2933, doi:10.1039/a902034i, 1999.

Chan, A. W. H., Kreisberg, N. M., Hohaus, T., Campuzano-Jost, P., Zhao, Y., Day, D. A., Kaser, L., Karl, T., Hansel, A., Teng, A. P., Ruehl, C. R., Sueper, D. T., Jayne, J. T., Worsnop, D. R., Jimenez, J. L., Hering, S. V., and Goldstein, A. H.: Speciated measurements of semivolatile and intermediate volatility organic compounds (S/IVOCs) in a pine forest during BEACHON-RoMBAS 2011, Atmos. Chem. Phys., 16, 1187–1205, doi:10.5194/acp-16-1187-2016, 2016.

Chen, Q., Liu, Y., Donahue, N. M., Shilling, J. E., and Martin, S. T.: Particle-phase chemistry of secondary organic material: modeled compared to measured $O:C$ and $H:C$ elemental ratios provide constraints, Environ. Sci. Technol., 45, 4763–4770, doi:10.1021/es104398s, 2011.

Chen, Q., Li, Y. L., McKinney, K. A., Kuwata, M., and Martin, S. T.: Particle mass yield from β-caryophyllene ozonolysis, Atmos. Chem. Phys., 12, 3165–3179, doi:10.5194/acp-12-3165-2012, 2012.

Chen, Q., Heald, C. L., Jimenez, J. L., Canagaratna, M. R., Zhang, Q., He, L., Huang, X.-F., Campuzano-Jost, P., Palm, B. B., Poulain, L., Kuwata, M., Martin, S. T., Abbatt, J. P. D., Lee, A. K. Y., and Liggio, J.: Elemental composition of organic aerosol: The gap between ambient and laboratory measurements, Geophys. Res. Lett., 42, 4182–4189, doi:10.1002/2015GL063693, 2015.

Chew, A. A., Atkinson, R., and Aschmann, S. M.: Kinetics of the gas-phase reactions of NO_3 radicals with a series of alcohols, glycol ethers, ethers and chloroalkenes, J. Chem. Soc. Trans., 94, 1083–1089, 1998.

Chhabra, P. S., Ng, N. L., Canagaratna, M. R., Corrigan, A. L., Russell, L. M., Worsnop, D. R., Flagan, R. C., and Seinfeld, J. H.: Elemental composition and oxidation of chamber organic aerosol, Atmos. Chem. Phys., 11, 8827–8845, doi:10.5194/acp-11-8827-2011, 2011.

Crounse, J. D., Nielsen, L. B., Jørgensen, S., Kjaergaard, H. G., and Wennberg, P. O.: Autoxidation of Organic Compounds in the Atmosphere, J. Phys. Chem. Lett., 4, 3513–3520, doi:10.1021/jz4019207, 2013.

Crump, J. G. and Seinfeld, J. H.: Turbulent deposition and gravitational sedimentation of an aerosol in a vessel of arbitrary shape, J. Aerosol Sci., 12, 405–415, doi:10.1016/0021-8502(81)90036-7, 1981.

Cubison, M. J., Ortega, A. M., Hayes, P. L., Farmer, D. K., Day, D., Lechner, M. J., Brune, W. H., Apel, E., Diskin, G. S., Fisher, J. A., Fuelberg, H. E., Hecobian, A., Knapp, D. J., Mikoviny, T., Riemer, D., Sachse, G. W., Sessions, W., Weber, R. J., Weinheimer, A. J., Wisthaler, A., and Jimenez, J. L.: Effects of aging on organic aerosol from open biomass burning smoke in aircraft and laboratory studies, Atmos. Chem. Phys., 11, 12049–12064, doi:10.5194/acp-11-12049-2011, 2011.

Day, D. A., Campuzano-Jost, P., Palm, B. B., Hu, W. W., Nault, B. A., Wooldridge, P. J., Cohen, R. C., Docherty, K. S., Huffman, J. A., and Jimenez, J. L.: Evaluation of methods for quantification of bulk particle-phase organic nitrates using real-time aerosol mass spectrometry, in preparation, 2017.

DeCarlo, P. F., Kimmel, J. R., Trimborn, A., Northway, M. J., Jayne, J. T., Aiken, A. C., Gonin, M., Fuhrer, K., Horvath, T., Docherty, K. S., Worsnop, D. R., and Jimenez, J. L.: Field-Deployable, High-Resolution, Time-of-Flight Aerosol Mass Spectrometer, Anal. Chem., 78, 8281–8289, doi:10.1021/ac061249n, 2006.

Farmer, D. K. and Cohen, R. C.: Observations of HNO_3, SAN, SPN and NO_2 fluxes: evidence for rapid HO_x chemistry within α pine forest canopy, Atmos. Chem. Phys., 8, 3899–3917, doi:10.5194/acp-8-3899-2008, 2008.

Farmer, D. K., Matsunaga, A., Docherty, K. S., Surratt, J. D., Seinfeld, J. H., Ziemann, P. J., and Jimenez, J. L.: Response of an aerosol mass spectrometer to organonitrates and organosulfates and implications for atmospheric chemistry, P. Natl. Acad. Sci. USA, 107, 6670–6675, doi:10.1073/pnas.0912340107, 2010.

Fry, J. L., Kiendler-Scharr, A., Rollins, A. W., Wooldridge, P. J., Brown, S. S., Fuchs, H., Dubé, W., Mensah, A., dal Maso, M., Tillmann, R., Dorn, H.-P., Brauers, T., and Cohen, R. C.: Organic nitrate and secondary organic aerosol yield from $NO3$ oxidation of β-pinene evaluated using a gas-phase kinetics/aerosol partitioning model, Atmos. Chem. Phys., 9, 1431–1449, doi:10.5194/acp-9-1431-2009, 2009.

Fry, J. L., Kiendler-Scharr, A., Rollins, A. W., Brauers, T., Brown, S. S., Dorn, H.-P., Dubé, W. P., Fuchs, H., Mensah, A., Rohrer, F., Tillmann, R., Wahner, A., Wooldridge, P. J., and Cohen, R. C.: SOA from limonene: role of $NO3$ in its generation and degradation, Atmos. Chem. Phys., 11, 3879–3894, doi:10.5194/acp-11-3879-2011, 2011.

Fry, J. L., Draper, D. C., Zarzana, K. J., Campuzano-Jost, P., Day, D. A., Jimenez, J. L., Brown, S. S., Cohen, R. C., Kaser, L., Hansel, A., Cappellin, L., Karl, T., Hodzic Roux, A., Turnipseed, A., Cantrell, C., Lefer, B. L., and Grossberg, N.: Observations of gas- and aerosol-phase organic nitrates at BEACHON-RoMBAS 2011, Atmos. Chem. Phys., 13, 8585–8605, doi:10.5194/acp-13-8585-2013, 2013.

Fry, J. L., Draper, D. C., Barsanti, K. C., Smith, J. N., Ortega, J., Winkler, P. M., Lawler, M. J., Brown, S. S., Edwards, P. M., Cohen, R. C., and Lee, L.: Secondary Organic Aerosol Formation and Organic Nitrate Yield from NO_3 Oxidation of Biogenic Hydrocarbons, Environ. Sci. Technol., 48, 11944–11953, doi:10.1021/es502204x, 2014.

George, I. J. and Abbatt, J. P. D.: Heterogeneous oxidation of atmospheric aerosol particles by gas-phase radicals, Nat. Chem., 2, 713–722, doi:10.1038/nchem.806, 2010.

George, I. J., Slowik, J., and Abbatt, J. P. D.: Chemical aging of ambient organic aerosol from heterogeneous reaction with hydroxyl radicals, Geophys. Res. Lett., 35, L13811, doi:10.1029/2008GL033884, 2008.

de Gouw, J. A. and Lovejoy, E. R.: Reactive uptake of ozone by liquid organic compounds, Geophys. Res. Lett., 25, 931–934, doi:10.1029/98GL00515, 1998.

Hallquist, M., Wängberg, I., Ljungström, E., Barnes, I., and Becker, K.-H.: Aerosol and product yields from NO_3 radical-initiated oxidation of selected monoterpenes, Environ. Sci. Technol., 33, 553–559, doi:10.1021/es980292s, 1999.

Hallquist, M., Wenger, J. C., Baltensperger, U., Rudich, Y., Simpson, D., Claeys, M., Dommen, J., Donahue, N. M., George, C., Goldstein, A. H., Hamilton, J. F., Herrmann, H., Hoffmann, T., Iinuma, Y., Jang, M., Jenkin, M. E., Jimenez, J. L., Kiendler-Scharr, A., Maenhaut, W., McFiggans, G., Mentel, Th. F., Monod, A., Prévôt, A. S. H., Seinfeld, J. H., Surratt, J. D., Szmigielski, R., and Wildt, J.: The formation, properties and impact of secondary organic aerosol: current and emerging issues, Atmos. Chem. Phys., 9, 5155–5236, doi:10.5194/acp-9-5155-2009, 2009.

Hayes, P. L., Carlton, A. G., Baker, K. R., Ahmadov, R., Washenfelder, R. A., Alvarez, S., Rappenglück, B., Gilman, J. B., Kuster, W. C., de Gouw, J. A., Zotter, P., Prévôt, A. S. H., Szidat, S., Kleindienst, T. E., Offenberg, J. H., Ma, P. K., and Jimenez, J. L.: Modeling the formation and aging of secondary organic aerosols in Los Angeles during CalNex 2010, Atmos. Chem. Phys., 15, 5773–5801, doi:10.5194/acp-15-5773-2015, 2015.

Heald, C. L., Kroll, J. H., Jimenez, J. L., Docherty, K. S., DeCarlo, P. F., Aiken, A. C., Chen, Q., Martin, S. T., Farmer, D. K., and Artaxo, P.: A simplified description of the evolution of organic aerosol composition in the atmosphere, Geophys. Res. Lett., 37, L08803, doi:10.1029/2010gl042737, 2010.

Hildebrandt Ruiz, L., Paciga, A. L., Cerully, K. M., Nenes, A., Donahue, N. M., and Pandis, S. N.: Formation and aging of secondary organic aerosol from toluene: changes in chemical composition, volatility, and hygroscopicity, Atmos. Chem. Phys., 15, 8301–8313, doi:10.5194/acp-15-8301-2015, 2015.

Hu, W., Palm, B. B., Day, D. A., Campuzano-Jost, P., Krechmer, J. E., Peng, Z., de Sá, S. S., Martin, S. T., Alexander, M. L., Baumann, K., Hacker, L., Kiendler-Scharr, A., Koss, A. R., de Gouw, J. A., Goldstein, A. H., Seco, R., Sjostedt, S. J., Park, J.-H., Guenther, A. B., Kim, S., Canonaco, F., Prévôt, A. S. H., Brune, W. H., and Jimenez, J. L.: Volatility and lifetime against OH heterogeneous reaction of ambient isoprene-epoxydiols-derived secondary organic aerosol (IEPOX-SOA), Atmos. Chem. Phys., 16, 11563–11580, doi:10.5194/acp-16-11563-2016, 2016.

Iannone, R., Xiao, S., and Bertram, A. K.: Potentially important nighttime heterogeneous chemistry: NO_3 with aldehydes and N_2O_5 with alcohols, Phys. Chem. Chem. Phys., 13, 10214, doi:10.1039/c1cp20294d, 2011.

Jaoui, M., Leungsakul, S., and Kamens, R. M.: Gas and Particle Products Distribution from the Reaction of β-Caryophyllene with Ozone, J. Atmos. Chem., 45, 261–287, doi:10.1023/A:1024263430285, 2003.

Jaoui, M., Kleindienst, T. E., Docherty, K. S., Lewandowski, M., and Offenberg, J. H.: Secondary organic aerosol formation from the oxidation of a series of sesquiterpenes: α-cedrene, β-caryophyllene, α-humulene and α-farnesene with O_3, OH and

NO_3 radicals, Environ. Chem., 10, 178, doi:10.1071/EN13025, 2013.

Jimenez, J. L., Canagaratna, M. R., Donahue, N. M., Prevot, A. S. H., Zhang, Q., Kroll, J. H., DeCarlo, P. F., Allan, J. D., Coe, H., Ng, N. L., Aiken, A. C., Docherty, K. S., Ulbrich, I. M., Grieshop, A. P., Robinson, A. L., Duplissy, J., Smith, J. D., Wilson, K. R., Lanz, V. A., Hueglin, C., Sun, Y. L., Tian, J., Laaksonen, A., Raatikainen, T., Rautiainen, J., Vaattovaara, P., Ehn, M., Kulmala, M., Tomlinson, J. M., Collins, D. R., Cubison, M. J., Dunlea, J., Huffman, J. A., Onasch, T. B., Alfarra, M. R., Williams, P. I., Bower, K., Kondo, Y., Schneider, J., Drewnick, F., Borrmann, S., Weimer, S., Demerjian, K., Salcedo, D., Cottrell, L., Griffin, R., Takami, A., Miyoshi, T., Hatakeyama, S., Shimono, A., Sun, J. Y., Zhang, Y. M., Dzepina, K., Kimmel, J. R., Sueper, D., Jayne, J. T., Herndon, S. C., Trimborn, A. M., Williams, L. R., Wood, E. C., Middlebrook, A. M., Kolb, C. E., Baltensperger, U., and Worsnop, D. R.: Evolution of Organic Aerosols in the Atmosphere, Science, 326, 1525–1529, doi:10.1126/science.1180353, 2009.

Kahnt, A., Iinuma, Y., Mutzel, A., Böge, O., Claeys, M., and Herrmann, H.: Campholenic aldehyde ozonolysis: a mechanism leading to specific biogenic secondary organic aerosol constituents, Atmos. Chem. Phys., 14, 719–736, doi:10.5194/acp-14-719-2014, 2014.

Kang, E., Root, M. J., Toohey, D. W., and Brune, W. H.: Introducing the concept of Potential Aerosol Mass (PAM), Atmos. Chem. Phys., 7, 5727–5744, doi:10.5194/acp-7-5727-2007, 2007.

Kang, E., Toohey, D. W., and Brune, W. H.: Dependence of SOA oxidation on organic aerosol mass concentration and OH exposure: experimental PAM chamber studies, Atmos. Chem. Phys., 11, 1837–1852, doi:10.5194/acp-11-1837-2011, 2011.

Kang, H., Day, D. A., Krechmer, J. E., Ayres, B. R., Keehan, N. I., Thompson, S. L., Hu, W., Campuzano-Jost, P., Schroder, J. C., Stark, H., Ranney, A. P., Ziemann, P. J., Zarzana, K. J., Wild, R. J., Dube, W. P., Brown, S. S., Fry, J. L., and Jimenez, J. L.: A33E-0280: Secondary organic aerosol mass yields from the dark NO_3 oxidation of α-pinene and Δ-carene: effect of RO_2 radical fate, in American Geophysical Union Fall Meeting, 2016.

Karjalainen, P., Timonen, H., Saukko, E., Kuuluvainen, H., Saarikoski, S., Aakko-Saksa, P., Murtonen, T., Bloss, M., Dal Maso, M., Simonen, P., Ahlberg, E., Svenningsson, B., Brune, W. H., Hillamo, R., Keskinen, J., and Rönkkö, T.: Time-resolved characterization of primary particle emissions and secondary particle formation from a modern gasoline passenger car, Atmos. Chem. Phys., 16, 8559–8570, doi:10.5194/acp-16-8559-2016, 2016.

Karl, T., Hansel, A., Cappellin, L., Kaser, L., Herdlinger-Blatt, I., and Jud, W.: Selective measurements of isoprene and 2-methyl-3-buten-2-ol based on NO^+ ionization mass spectrometry, Atmos. Chem. Phys., 12, 11877–11884, doi:10.5194/acp-12-11877-2012, 2012.

Kaser, L., Karl, T., Schnitzhofer, R., Graus, M., Herdlinger-Blatt, I. S., DiGangi, J. P., Sive, B., Turnipseed, A., Hornbrook, R. S., Zheng, W., Flocke, F. M., Guenther, A., Keutsch, F. N., Apel, E., and Hansel, A.: Comparison of different real time VOC measurement techniques in a ponderosa pine forest, Atmos. Chem. Phys., 13, 2893–2906, doi:10.5194/acp-13-2893-2013, 2013.

Keller, A. and Burtscher, H.: A continuous photo-oxidation flow reactor for a defined measurement of the SOA formation po-

tential of wood burning emissions, J. Aerosol Sci., 49, 9–20, doi:10.1016/j.jaerosci.2012.02.007, 2012.

Kim, S., Karl, T., Guenther, A., Tyndall, G., Orlando, J., Harley, P., Rasmussen, R., and Apel, E.: Emissions and ambient distributions of Biogenic Volatile Organic Compounds (BVOC) in a ponderosa pine ecosystem: interpretation of PTR-MS mass spectra, Atmos. Chem. Phys., 10, 1759–1771, doi:10.5194/acp-10-1759-2010, 2010.

Kim, S., Wolfe, G. M., Mauldin, L., Cantrell, C., Guenther, A., Karl, T., Turnipseed, A., Greenberg, J., Hall, S. R., Ullmann, K., Apel, E., Hornbrook, R., Kajii, Y., Nakashima, Y., Keutsch, F. N., DiGangi, J. P., Henry, S. B., Kaser, L., Schnitzhofer, R., Graus, M., Hansel, A., Zheng, W., and Flocke, F. F.: Evaluation of HOx sources and cycling using measurement-constrained model calculations in a 2-methyl-3-buten-2-ol (MBO) and monoterpene (MT) dominated ecosystem, Atmos. Chem. Phys., 13, 2031–2044, doi:10.5194/acp-13-2031-2013, 2013.

Knap, H. C., Schmidt, J. A., and Jørgensen, S.: Hydrogen shift reactions in four methyl-buten-ol (MBO) peroxy radicals and their impact on the atmosphere, Atmos. Environ., 147, 79–87, doi:10.1016/j.atmosenv.2016.09.064, 2016.

Knote, C., Hodzic, A., and Jimenez, J. L.: The effect of dry and wet deposition of condensable vapors on secondary organic aerosols concentrations over the continental US, Atmos. Chem. Phys., 15, 1–18, doi:10.5194/acp-15-1-2015, 2015.

Krechmer, J. E., Coggon, M. M., Massoli, P., Nguyen, T. B., Crounse, J. D., Hu, W., Day, D. A., Tyndall, G. S., Henze, D. K., Rivera-Rios, J. C., Nowak, J. B., Kimmel, J. R., Mauldin, R. L., Stark, H., Jayne, J. T., Sipilä, M., Junninen, H., Clair, J. M. St., Zhang, X., Feiner, P. A., Zhang, L., Miller, D. O., Brune, W. H., Keutsch, F. N., Wennberg, P. O., Seinfeld, J. H., Worsnop, D. R., Jimenez, J. L., and Canagaratna, M. R.: Formation of Low Volatility Organic Compounds and Secondary Organic Aerosol from Isoprene Hydroxyhydroperoxide Low-NO Oxidation, Environ. Sci. Technol., 49, 10330–10339, doi:10.1021/acs.est.5b02031, 2015.

Kroll, J. H. and Seinfeld, J. H.: Chemistry of secondary organic aerosol: Formation and evolution of low-volatility organics in the atmosphere, Atmos. Environ., 42, 3593–3624, doi:10.1016/j.atmosenv.2008.01.003, 2008.

Kroll, J. H., Donahue, N. M., Jimenez, J. L., Kessler, S. H., Canagaratna, M. R., Wilson, K. R., Altieri, K. E., Mazzoleni, L. R., Wozniak, A. S., Bluhm, H., Mysak, E. R., Smith, J. D., Kolb, C. E., and Worsnop, D. R.: Carbon oxidation state as a metric for describing the chemistry of atmospheric organic aerosol, Nat. Chem., 3, 133–139, doi:10.1038/nchem.948, 2011.

Kuwata, M., Zorn, S. R., and Martin, S. T.: Using elemental ratios to predict the density of organic material composed of carbon, hydrogen, and oxygen., Environ. Sci. Technol., 46, 787–94, doi:10.1021/es202525q, 2012.

La, Y. S., Camredon, M., Ziemann, P. J., Valorso, R., Matsunaga, A., Lannuque, V., Lee-Taylor, J., Hodzic, A., Madronich, S., and Aumont, B.: Impact of chamber wall loss of gaseous organic compounds on secondary organic aerosol formation: explicit modeling of SOA formation from alkane and alkene oxidation, Atmos. Chem. Phys., 16, 1417–1431, doi:10.5194/acp-16-1417-2016, 2016.

Lambe, A. T., Onasch, T. B., Massoli, P., Croasdale, D. R., Wright, J. P., Ahern, A. T., Williams, L. R., Worsnop, D. R., Brune, W. H., and Davidovits, P.: Laboratory studies of the chemical composition and cloud condensation nuclei (CCN) activity of secondary organic aerosol (SOA) and oxidized primary organic aerosol (OPOA), Atmos. Chem. Phys., 11, 8913–8928, doi:10.5194/acp-11-8913-2011, 2011.

Lambe, A. T., Onasch, T. B., Croasdale, D. R., Wright, J. P., Martin, A. T., Franklin, J. P., Massoli, P., Kroll, J. H., Canagaratna, M. R., Brune, W. H., Worsnop, D. R., and Davidovits, P.: Transitions from Functionalization to Fragmentation Reactions of Laboratory Secondary Organic Aerosol (SOA) Generated from the OH Oxidation of Alkane Precursors, Environ. Sci. Technol., 46, 5430–5437, doi:10.1021/es300274t, 2012.

Lambe, A. T., Ahern, A. T., Wright, J. P., Croasdale, D. R., Davidovits, P., and Onasch, T. B.: Oxidative aging and cloud condensation nuclei activation of laboratory combustion soot, J. Aerosol Sci., 79, 31–39, doi:10.1016/j.jaerosci.2014.10.001, 2014.

Lambe, A. T., Chhabra, P. S., Onasch, T. B., Brune, W. H., Hunter, J. F., Kroll, J. H., Cummings, M. J., Brogan, J. F., Parmar, Y., Worsnop, D. R., Kolb, C. E., and Davidovits, P.: Effect of oxidant concentration, exposure time, and seed particles on secondary organic aerosol chemical composition and yield, Atmos. Chem. Phys., 15, 3063–3075, doi:10.5194/acp-15-3063-2015, 2015.

Lee, A., Goldstein, A. H., Kroll, J. H., Ng, N. L., Varutbangkul, V., Flagan, R. C., and Seinfeld, J. H.: Gas-phase products and secondary aerosol yields from the photooxidation of 16 different terpenes, J. Geophys. Res., 111, D17305, doi:10.1029/2006JD007050, 2006.

Li, R., Palm, B. B., Borbon, A., Graus, M., Warneke, C., Ortega, A. M., Day, D. A., Brune, W. H., Jimenez, J. L., de Gouw, J. A., and Brune, B.: Laboratory studies on secondary organic aerosol formation from crude oil vapors, Environ. Sci. Technol., 47, 12566–12574, doi:10.1021/es402265y, 2013.

Li, R., Palm, B. B., Ortega, A. M., Hlywiak, J., Hu, W., Peng, Z., Day, D. A., Knote, C., Brune, W. H., de Gouw, J. A., and Jimenez, J. L.: Modeling the Radical Chemistry in an Oxidation Flow Reactor: Radical Formation and Recycling, Sensitivities, and the OH Exposure Estimation Equation, J. Phys. Chem. A, 119, 4418–4432, doi:10.1021/jp509534k, 2015.

Liu, S., Shilling, J. E., Song, C., Hiranuma, N., Zaveri, R. A., and Russell, L. M.: Hydrolysis of Organonitrate Functional Groups in Aerosol Particles, Aerosol Sci. Technol., 46, 1359–1369, doi:10.1080/02786826.2012.716175, 2012.

Massoli, P., Lambe, A. T., Ahern, A. T., Williams, L. R., Ehn, M., Mikkilä, J., Canagaratna, M. R., Brune, W. H., Onasch, T. B., Jayne, J. T., Petäjä, T., Kulmala, M., Laaksonen, A., Kolb, C. E., Davidovits, P., and Worsnop, D. R.: Relationship between aerosol oxidation level and hygroscopic properties of laboratory generated secondary organic aerosol (SOA) particles, Geophys. Res. Lett., 37, L24801, doi:10.1029/2010GL045258, 2010.

Matsunaga, A. and Ziemann, P. J.: Gas-Wall Partitioning of Organic Compounds in a Teflon Film Chamber and Potential Effects on Reaction Product and Aerosol Yield Measurements, Aerosol Sci. Technol., 44, 881–892, doi:10.1080/02786826.2010.501044, 2010.

McMurry, P. H. and Rader, D. J.: Aerosol Wall Losses in Electrically Charged Chambers, Aerosol Sci. Technol., 4, 249–268, doi:10.1080/02786828508959054, 1985.

Moldanova, J. and Ljungström, E.: Modeling of particle formation from NO$_3$ oxidation of selected monoterpenes, J. Aerosol Sci., 31, 1317–1333, doi:10.1016/S0021-8502(00)00041-0, 2000.

Morris, J. W., Davidovits, P., Jayne, J. T., Jimenez, J. L., Shi, Q., Kolb, C. E., Worsnop, D. R., Barney, W. S., and Cass, G.: Kinetics of submicron oleic acid aerosols with ozone: A novel aerosol mass spectrometric technique, Geophys. Res. Lett., 29, 71-1–71-4, doi:10.1029/2002GL014692, 2002.

Myhre, G., Shindell, D., Bréon, F.-M., Collins, W., Fuglestvedt, J., Huang, J., Koch, D., Lamarque, J.-F., Lee, D., Mendoza, B., Nakajima, T., Robock, A., Stephens, G., Takemura, T., and Zhang, H.: Anthropogenic and Natural Radiative Forcing, in Climate Change 2013: The Physical Science Basis. Contribution of Working Group I to the Fifth Assessment Report of the Intergovernmental Panel on Climate Change, edited by: Stocker, T. F., Qin, D., Plattner, G.-K., Tignor, M., Allen, S. K., Boschung, J., Nauels, A., Xia, Y., Bex, V., and Midgley, P. M., Cambridge University Press, Cambridge, UK, New York, NY, USA, 659–740, 2013.

Nah, T., McVay, R. C., Zhang, X., Boyd, C. M., Seinfeld, J. H., and Ng, N. L.: Influence of seed aerosol surface area and oxidation rate on vapor wall deposition and SOA mass yields: a case study with a-pinene ozonolysis, Atmos. Chem. Phys., 16, 9361–9379, doi:10.5194/acp-16-9361-2016, 2016.

Ng, N. L., Kroll, J. H., Keywood, M. D., Bahreini, R., Varutbangkul, V., Flagan, R. C., Seinfeld, J. H., Lee, A., and Goldstein, A. H.: Contribution of first- versus second-generation products to secondary organic aerosols formed in the oxidation of biogenic hydrocarbons, Environ. Sci. Technol., 40, 2283–2297, doi:10.1021/es052269u, 2006.

Ng, N. L., Canagaratna, M. R., Jimenez, J. L., Chhabra, P. S., Seinfeld, J. H., and Worsnop, D. R.: Changes in organic aerosol composition with aging inferred from aerosol mass spectra, Atmos. Chem. Phys., 11, 6465–6474, doi:10.5194/acp-11-6465-2011, 2011.

Ng, N. L., Brown, S. S., Archibald, A. T., Atlas, E., Cohen, R. C., Crowley, J. N., Day, D. A., Donahue, N. M., Fry, J. L., Fuchs, H., Griffin, R. J., Guzman, M. I., Herrmann, H., Hodzic, A., Iinuma, Y., Jimenez, J. L., Kiendler-Scharr, A., Lee, B. H., Luecken, D. J., Mao, J., McLaren, R., Mutzel, A., Osthoff, H. D., Ouyang, B., Picquet-Varrault, B., Platt, U., Pye, H. O. T., Rudich, Y., Schwantes, R. H., Shiraiwa, M., Stutz, J., Thornton, J. A., Tilgner, A., Williams, B. J., and Zaveri, R. A.: Nitrate radicals and biogenic volatile organic compounds: oxidation, mechanisms, and organic aerosol, Atmos. Chem. Phys., 17, 2103–2162, doi:10.5194/acp-17-2103-2017, 2017.

Nguyen, T. B., Crounse, J. D., Teng, A. P., St. Clair, J. M., Paulot, F., Wolfe, G. M., and Wennberg, P. O.: Rapid deposition of oxidized biogenic compounds to a temperate forest, P. Natl. Acad. Sci. USA, 112, E392–E401, doi:10.1073/pnas.1418702112, 2015.

Orlando, J. J. and Tyndall, G. S.: Laboratory studies of organic peroxy radical chemistry: an overview with emphasis on recent issues of atmospheric significance, Chem. Soc. Rev., 41, 6294, doi:10.1039/c2cs35166h, 2012.

Ortega, A. M., Day, D. A., Cubison, M. J., Brune, W. H., Bon, D., de Gouw, J. A., and Jimenez, J. L.: Secondary organic aerosol formation and primary organic aerosol oxidation from biomass-burning smoke in a flow reactor during FLAME-3, Atmos. Chem. Phys., 13, 11551–11571, doi:10.5194/acp-13-11551-2013, 2013.

Ortega, A. M., Hayes, P. L., Peng, Z., Palm, B. B., Hu, W., Day, D. A., Li, R., Cubison, M. J., Brune, W. H., Graus, M., Warneke, C., Gilman, J. B., Kuster, W. C., de Gouw, J., Gutiérrez-Montes, C., and Jimenez, J. L.: Real-time measurements of secondary organic aerosol formation and aging from ambient air in an oxidation flow reactor in the Los Angeles area, Atmos. Chem. Phys., 16, 7411–7433, doi:10.5194/acp-16-7411-2016, 2016.

Ortega, J., Turnipseed, A., Guenther, A. B., Karl, T. G., Day, D. A., Gochis, D., Huffman, J. A., Prenni, A. J., Levin, E. J. T., Kreidenweis, S. M., DeMott, P. J., Tobo, Y., Patton, E. G., Hodzic, A., Cui, Y. Y., Harley, P. C., Hornbrook, R. S., Apel, E. C., Monson, R. K., Eller, A. S. D., Greenberg, J. P., Barth, M. C., Campuzano-Jost, P., Palm, B. B., Jimenez, J. L., Aiken, A. C., Dubey, M. K., Geron, C., Offenberg, J., Ryan, M. G., Fornwalt, P. J., Pryor, S. C., Keutsch, F. N., DiGangi, J. P., Chan, A. W. H., Goldstein, A. H., Wolfe, G. M., Kim, S., Kaser, L., Schnitzhofer, R., Hansel, A., Cantrell, C. A., Mauldin, R. L., and Smith, J. N.: Overview of the Manitou Experimental Forest Observatory: site description and selected science results from 2008 to 2013, Atmos. Chem. Phys., 14, 6345–6367, doi:10.5194/acp-14-6345-2014, 2014.

Palm, B. B., Campuzano-Jost, P., Ortega, A. M., Day, D. A., Kaser, L., Jud, W., Karl, T., Hansel, A., Hunter, J. F., Cross, E. S., Kroll, J. H., Peng, Z., Brune, W. H., and Jimenez, J. L.: In situ secondary organic aerosol formation from ambient pine forest air using an oxidation flow reactor, Atmos. Chem. Phys., 16, 2943–2970, doi:10.5194/acp-16-2943-2016, 2016.

Pathak, R., Donahue, N. M., and Pandis, S. N.: Ozonolysis of β-Pinene: Temperature Dependence of Secondary Organic Aerosol Mass Fraction, Environ. Sci. Technol., 42, 5081–5086, doi:10.1021/es070721z, 2008.

Pathak, R. K., Presto, A. A., Lane, T. E., Stanier, C. O., Donahue, N. M., and Pandis, S. N.: Ozonolysis of α-pinene: parameterization of secondary organic aerosol mass fraction, Atmos. Chem. Phys., 7, 3811–3821, doi:10.5194/acp-7-3811-2007, 2007.

Peng, Z., Day, D. A., Stark, H., Li, R., Lee-Taylor, J., Palm, B. B., Brune, W. H., and Jimenez, J. L.: HO$_x$ radical chemistry in oxidation flow reactors with low-pressure mercury lamps systematically examined by modeling, Atmos. Meas. Tech., 8, 4863–4890, doi:10.5194/amt-8-4863-2015, 2015.

Peng, Z., Day, D. A., Ortega, A. M., Palm, B. B., Hu, W., Stark, H., Li, R., Tsigaridis, K., Brune, W. H., and Jimenez, J. L.: Non-OH chemistry in oxidation flow reactors for the study of atmospheric chemistry systematically examined by modeling, Atmos. Chem. Phys., 16, 4283–4305, doi:10.5194/acp-16-4283-2016, 2016.

Pierce, J. R., Engelhart, G. J., Hildebrandt, L., Weitkamp, E. A., Pathak, R. K., Donahue, N. M., Robinson, A. L., Adams, P. J., and Pandis, S. N.: Constraining Particle Evolution from Wall Losses, Coagulation, and Condensation-Evaporation in Smog-Chamber Experiments: Optimal Estimation Based on Size Distribution Measurements, Aerosol Sci. Technol., 42, 1001–1015, doi:10.1080/02786820802389251, 2008.

Pope, C. A. and Dockery, D. W.: Health Effects of Fine Particulate Air Pollution: Lines that Connect, J. Air Waste Manage. Assoc., 56, 709–742, doi:10.1080/10473289.2006.10464485, 2006.

Richters, S., Herrmann, H. and Berndt, T.: Gas-phase rate coefficients of the reaction of ozone with four sesquiterpenes

at 295 ± 2 K, Phys. Chem. Chem. Phys., 17, 11658–11669, doi:10.1039/C4CP05542J, 2015.

Rogge, W. F., Hildemann, L. M., Mazurek, M. A., Cass, G. R., and Simoneit, B. R. T.: Sources of fine organic aerosol. 1. Charbroilers and meat cooking operations, Environ. Sci. Technol., 25, 1112–1125, doi:10.1021/es00018a015, 1991.

Saukko, E., Lambe, A. T., Massoli, P., Koop, T., Wright, J. P., Croasdale, D. R., Pedernera, D. A., Onasch, T. B., Laaksonen, A., Davidovits, P., Worsnop, D. R., and Virtanen, A.: Humidity-dependent phase state of SOA particles from biogenic and anthropogenic precursors, Atmos. Chem. Phys., 12, 7517–7529, doi:10.5194/acp-12-7517-2012, 2012.

Shilling, J. E., Chen, Q., King, S. M., Rosenoern, T., Kroll, J. H., Worsnop, D. R., McKinney, K. A., and Martin, S. T.: Particle mass yield in secondary organic aerosol formed by the dark ozonolysis of α-pinene, Atmos. Chem. Phys., 8, 2073–2088, doi:10.5194/acp-8-2073-2008, 2008.

Shrivastava, M., Thornton, J., Cappa, C., Fan, J., Goldstein, A., Guenther, A., Jimenez, J. L., Kuang, C., Laskin, A., Martin, S., Ng, N. L., Petaja, T., Pierce, J., Rasch, P., Roldin, P., Seinfeld, J., Shilling, J., Smith, J., Volkamer, R., Wang, J., Worsnop, D., Zaveri, R., Zelenyuk, A., and Zhang, Q.: Recent advances in understanding secondary organic aerosols: implications for global climate forcing, Rev. Geophys., revised, 2016.

Smith, J. D., Kroll, J. H., Cappa, C. D., Che, D. L., Liu, C. L., Ahmed, M., Leone, S. R., Worsnop, D. R., and Wilson, K. R.: The heterogeneous reaction of hydroxyl radicals with submicron squalane particles: a model system for understanding the oxidative aging of ambient aerosols, Atmos. Chem. Phys., 9, 3209–3222, doi:10.5194/acp-9-3209-2009, 2009.

Spittler, M., Barnes, I., Bejan, I., Brockmann, K. J., Benter, T., and Wirtz, K.: Reactions of NO$_3$ radicals with limonene and α-pinene: Product and SOA formation, Atmos. Environ., 40, 116–127, doi:10.1016/j.atmosenv.2005.09.093, 2006.

Tanaka, P. L., Allen, D. T., and Mullins, C. B.: An environmental chamber investigation of chlorine-enhanced ozone formation in Houston, Texas, J. Geophys. Res., 108, 4576, doi:10.1029/2002JD003314, 2003.

Tasoglou, A. and Pandis, S. N.: Formation and chemical aging of secondary organic aerosol during the β-caryophyllene oxidation, Atmos. Chem. Phys., 15, 6035–6046, doi:10.5194/acp-15-6035-2015, 2015.

Thornton, J. A., Wooldridge, P. J., and Cohen, R. C.: Atmospheric NO$_2$: In Situ Laser-Induced Fluorescence Detection at Parts per Trillion Mixing Ratios, Anal. Chem., 72, 528–539, doi:10.1021/ac9908905, 2000.

Timonen, H., Karjalainen, P., Saukko, E., Saarikoski, S., Aakko-Saksa, P., Simonen, P., Murtonen, T., Dal Maso, M., Kuuluvainen, H., Ahlberg, E., Svenningsson, B., Pagels, J., Brune, W. H., Keskinen, J., Worsnop, D. R., Hillamo, R., and Rönkkö, T.: Influence of fuel ethanol content on primary emissions and secondary aerosol formation potential for a modern flex-fuel gasoline vehicle, Atmos. Chem. Phys. Discuss., doi:10.5194/acp-2016-579, in review, 2016.

Tkacik, D. S., Lambe, A. T., Jathar, S., Li, X., Presto, A. A., Zhao, Y., Blake, D., Meinardi, S., Jayne, J. T., Croteau, P. L., and Robinson, A. L.: Secondary Organic Aerosol Formation from in-Use Motor Vehicle Emissions Using a Potential

Aerosol Mass Reactor, Environ. Sci. Technol., 48, 11235–11242, doi:10.1021/es502239v, 2014.

Tsigaridis, K., Daskalakis, N., Kanakidou, M., Adams, P. J., Artaxo, P., Bahadur, R., Balkanski, Y., Bauer, S. E., Bellouin, N., Benedetti, A., Bergman, T., Berntsen, T. K., Beukes, J. P., Bian, H., Carslaw, K. S., Chin, M., Curci, G., Diehl, T., Easter, R. C., Ghan, S. J., Gong, S. L., Hodzic, A., Hoyle, C. R., Iversen, T., Jathar, S., Jimenez, J. L., Kaiser, J. W., Kirkevåg, A., Koch, D., Kokkola, H., Lee, Y. H., Lin, G., Liu, X., Luo, G., Ma, X., Mann, G. W., Mihalopoulos, N., Morcrette, J.-J., Müller, J.-F., Myhre, G., Myriokefalitakis, S., Ng, N. L., O'Donnell, D., Penner, J. E., Pozzoli, L., Pringle, K. J., Russell, L. M., Schulz, M., Sciare, J., Seland, Ø., Shindell, D. T., Sillman, S., Skeie, R. B., Spracklen, D., Stavrakou, T., Steenrod, S. D., Takemura, T., Tiitta, P., Tilmes, S., Tost, H., van Noije, T., van Zyl, P. G., von Salzen, K., Yu, F., Wang, Z., Wang, Z., Zaveri, R. A., Zhang, H., Zhang, K., Zhang, Q., and Zhang, X.: The AeroCom evaluation and intercomparison of organic aerosol in global models, Atmos. Chem. Phys., 14, 10845–10895, doi:10.5194/acp-14-10845-2014, 2014.

Vereecken, L. and Peeters, J.: Enhanced H-atom abstraction from pinonaldehyde, pinonic acid, pinic acid, and related compounds: theoretical study of C–H bond strengths, Phys. Chem. Chem. Phys., 4, 467–472, doi:10.1039/b109370c, 2002.

Volkamer, R., Jimenez, J. L., San Martini, F., Dzepina, K., Zhang, Q., Salcedo, D., Molina, L. T., Worsnop, D. R., and Molina, M. J.: Secondary organic aerosol formation from anthropogenic air pollution: Rapid and higher than expected, Geophys. Res. Lett., 33, L17811, doi:10.1029/2006GL026899, 2006.

Wagner, N. L., Dubé, W. P., Washenfelder, R. A., Young, C. J., Pollack, I. B., Ryerson, T. B., and Brown, S. S.: Diode laser-based cavity ring-down instrument for NO$_3$, N$_2$O$_5$, NO, NO$_2$ and O$_3$ from aircraft, Atmos. Meas. Tech., 4, 1227–1240, doi:10.5194/amt-4-1227-2011, 2011.

Winterhalter, R., Herrmann, F., Kanawati, B., Nguyen, T. L., Peeters, J., Vereecken, L., and Moortgat, G. K.: The gas-phase ozonolysis of β-caryophyllene (C$_{15}$H$_{24}$). Part I: an experimental study, Phys. Chem. Chem. Phys., 11, 4152, doi:10.1039/b817824k, 2009.

Wolfe, G. M., Cantrell, C., Kim, S., Mauldin III, R. L., Karl, T., Harley, P., Turnipseed, A., Zheng, W., Flocke, F., Apel, E. C., Hornbrook, R. S., Hall, S. R., Ullmann, K., Henry, S. B., DiGangi, J. P., Boyle, E. S., Kaser, L., Schnitzhofer, R., Hansel, A., Graus, M., Nakashima, Y., Kajii, Y., Guenther, A., and Keutsch, F. N.: Missing peroxy radical sources within a summertime ponderosa pine forest, Atmos. Chem. Phys., 14, 4715–4732, doi:10.5194/acp-14-4715-2014, 2014.

Yu, J., Griffin, R. J., Cocker, D. R., Flagan, R. C., Seinfeld, J. H., and Blanchard, P.: Observation of gaseous and particulate products of monoterpene oxidation in forest atmospheres, Geophys. Res. Lett., 26, 1145–1148, doi:10.1029/1999GL900169, 1999.

Zhang, H., Worton, D. R., Lewandowski, M., Ortega, J., Rubitschun, C. L., Park, J.-H., Kristensen, K., Campuzano-Jost, P., Day, D. A., Jimenez, J. L., Jaoui, M., Offenberg, J. H., Kleindienst, T. E., Gilman, J., Kuster, W. C., de Gouw, J., Park, C., Schade, G. W., Frossard, A. A., Russell, L., Kaser, L., Jud, W., Hansel, A., Cappellin, L., Karl, T., Glasius, M., Guenther, A., Goldstein, A. H., Seinfeld, J. H., Gold, A., Kamens, R. M., and Surratt, J. D.: Organosulfates as Tracers for Secondary

Organic Aerosol (SOA) Formation from 2-Methyl-3-Buten-2-ol (MBO) in the Atmosphere, Environ. Sci. Technol., 46, 9437–9446, doi:10.1021/es301648z, 2012.

Zhang, Q., Jimenez, J. L., Canagaratna, M. R., Allan, J. D., Coe, H., Ulbrich, I., Alfarra, M. R., Takami, A., Middlebrook, A. M., Sun, Y. L., Dzepina, K., Dunlea, E., Docherty, K., De-Carlo, P. F., Salcedo, D., Onasch, T., Jayne, J. T., Miyoshi, T., Shimono, A., Hatakeyama, S., Takegawa, N., Kondo, Y., Schneider, J., Drewnick, F., Borrmann, S., Weimer, S., Demerjian, K., Williams, P., Bower, K., Bahreini, R., Cottrell, L., Griffin, R. J., Rautiainen, J., Sun, J. Y., Zhang, Y. M., and Worsnop, D. R.: Ubiquity and dominance of oxygenated species in organic aerosols in anthropogenically-influenced Northern Hemisphere midlatitudes, Geophys. Res. Lett., 34, L13801, doi:10.1029/2007GL029979, 2007.

Zhang, X., Cappa, C. D., Jathar, S. H., McVay, R. C., Ensberg, J. J., Kleeman, M. J., and Seinfeld, J. H.: Influence of vapor wall loss in laboratory chambers on yields of secondary organic aerosol, P. Natl. Acad. Sci. USA, 111, 5802–5807, doi:10.1073/pnas.1404727111, 2014.

Zhao, D. F., Kaminski, M., Schlag, P., Fuchs, H., Acir, I.-H., Bohn, B., Häseler, R., Kiendler-Scharr, A., Rohrer, F., Tillmann, R., Wang, M. J., Wegener, R., Wildt, J., Wahner, A., and Mentel, T. F.: Secondary organic aerosol formation from hydroxyl radical oxidation and ozonolysis of monoterpenes, Atmos. Chem. Phys., 15, 991–1012, doi:10.5194/acp-15-991-2015, 2015.

Ziemann, P. J.: Aerosol products, mechanisms, and kinetics of heterogeneous reactions of ozone with oleic acid in pure and mixed particles, Faraday Discuss., 130, 469, doi:10.1039/b417502f, 2005.